7-1-2003

Natural Superconvergent Points of Triangular Finite Elements

Zhimin Zhang
Wayne State University, zhimin.zhang@wayne.edu

Runchang Lin
Wayne State University

NATURAL SUPERCONVERGENT POINTS OF TRIANGULAR FINITE ELEMENTS

Zhimin Zhang and Runchang Lin

WAYNE STATE UNIVERSITY

Detroit, MI 48202

Department of Mathematics
Research Report

2003 Series
#7

This research was partly supported by the National Science Foundation.

Natural Superconvergent Points of Triangular Finite Elements

Zhimin Zhang* and Runchang Lin
Department of Mathematics, Wayne State University

Abstract. In this work, we analytically identify natural superconvergent points of function values and gradients for triangular elements. Both the Poisson equation and the Laplace equation are discussed for polynomial finite element spaces (with degrees up to 8) under four different mesh patterns. Our results verify computer findings of [2], especially, we confirm that the computed data have 9 digits of accuracy with an exception of one pair (which has 8-7 digits of accuracy). In addition, we demonstrate that the function value superconvergent points predicted by the symmetry theory [14] are the only superconvergent points for the Poisson equation. Finally, we provide function value superconvergent points for the Laplace equation, which are not reported elsewhere in the literature.

Key Words. Finite element method, natural superconvergence, triangular elements.

AMS Subject Classification. 65N30, 65N15

1. INTRODUCTION

Natural superconvergent points are special points where the convergence of numerical approximations exceeds the possible global rate without any post-processing. The investigation regarding the finite element superconvergence has a long history since 70' [6]. For the literature, the reader is referred to books [3, 4, 5, 9, 12, 17, 20] and references therein.

In mid-90', Babuška *et al.* developed a "computer-based proof" [2] that systematically predicted derivative superconvergent points for the Laplace equation, the Poisson equation, and linear elasticity equations. They considered four mesh patterns of triangular elements and three families of rectangular elements of degree n, $1 \leq n \leq 7$. Their investigation reduced the problem of finding superconvergent points to the problem of finding intersections of certain polynomial contours. The actual superconvergent points were located by computer programs without explicitly constructing those polynomials, and 10 digits were provided in their reported data [2, 3]. Later, Zhang proposed an analytic approach which constructs explicitly the needed polynomials through an orthogonal decomposition under local rectangular and brick meshes [18, 19]. His result confirmed that ten digits reported by computer findings are correct up to rounding with only one exception (8-accurate digits).

A parallel analytic approach for triangular meshes are much more involved and tedious, which will be the main object of the current investigation. We consider the Laplace and Poisson equations on the four triangular mesh patterns used in the computer-based proof. By a special orthogonal decomposition, we explicitly construct those polynomials from which the superconvergent points are located. Our results verify that the computed data

*This research was partially supported by the National Science Foundation grants DMS-0074301, DMS-0079743, and INT-0196139.

for triangular elements in [2] have 9 digits of accuracy except one pair (with 8-7 accurate digits). In addition, we report for the first time, superconvergent points for function values of the Laplace equation.

Another systematic way to find superconvergent points in mid-90' is the symmetry theory developed by Schatz *et al.* [14]. This theory predicts that superconvergence occurs at local mesh symmetry points for a large class of 2nd-order elliptic problems of any dimension. For odd order elements (linear, cubic, etc.), superconvergence happens to derivatives; and for even order elements (quadratic and so on), it is for function values. A by-product of our current work is to confirm that for the Poisson equation under triangular meshes, the mesh symmetry points are "almost" all superconvergent points.

An outline of this paper is as follows: Section 2 contains the main theorems which will reduce the problem of finding superconvergent points to that of finding intersections of certain polynomial contours. In Section 3, superconvergent points of function values and gradients of both the Poisson equation and the Laplace equation are provided for four patterns of triangular meshes. The main idea is illustrated in the beginning of Section 3.1 for the regular pattern. The detailed superconvergent points are provided in Sections 3.1–3.4, for four mesh patterns, respectively.

2. THEORETICAL SETTING

We shall outline the process by Babuška *et al.* [2] in finding derivative superconvergent points. Here we follow the description provided by Wahlbin [17].

The main hypotheses in [2] are: (a) there is no roundoff error; (b) the mesh is locally translation invariant; (c) the solution is sufficiently smooth locally and the pollution error is under control. Throughout this paper, we assume hypotheses (b) and (c). However, the hypothesis (a) is no longer needed, since the explicit expressions of involved polynomials are provided. Another advantage of this method is that it is easily repeated.

Let $\Omega \in \mathbb{R}^2$ be a bounded domain. Denote in general a square centered at $\mathbf{x} = (x_1, x_2)$ of side $2h$ as $c(\mathbf{x}, h) = \{\mathbf{y} = (y_1, y_2) \in \Omega \mid |y_i - x_i| \leq h,\ i = 1, 2\}$. Consider the local *natural*-superconvergent points near $\mathbf{x}^0 \in \Omega$. Let $c(\mathbf{x}^0, h)$ be the $2h \times 2h$ master cell. Let $\Omega_1 = c(\mathbf{x}^0, H)$ and $\Omega_0 = c(\mathbf{x}^0, 2H)$ be two squares in Ω with $H = h^\delta$, $0 < \delta < 1$, such that the $2h$-periodic extensions of the master cell fit them exactly. Assume that a finite element approximation $u_h \in S_h(\Omega_0)$ of u, the solution of a Poisson equation, satisfies

$$D(u - u_h, v) = 0, \quad \forall v \in S_h^{comp}(\Omega_0), \tag{2.1}$$

where $D(w, v) = \int \nabla w \cdot \nabla v$, $S_h^{comp}(\Omega_0)$ is the finite element subspace which has compact support on Ω_0. We shall assume that

$$\|u - u_h\|_{L_\infty(\Omega_0)} \leq C h^{n+1-L}, \tag{2.2}$$

with $L \geq 0$ and $L + \delta < 1$. This assumption implies that pollution effects from outside of the domain Ω_0 have been properly controlled and the error loss is of order h^L. Moreover, we may assume that

$$\|u - u_h\|_{W_\infty^{-1}(\Omega_0)} \leq C h^{n+2-\Lambda}, \tag{2.3}$$

with $\Lambda \geq 0$ and $\Lambda + \delta < 1$.

Under various conditions given in [15], we have

Lemma 2.1. *Let u and u_h satisfy (2.1). Then for each $s \geq 0$ and $1 \leq q \leq \infty$ there exists a constant C independent of u, u_h, h, H, and $\mathbf{x}^0$ such that*

$$\begin{aligned}\|u - u_h\|_{W^1_\infty(\Omega_1)} &\leq C \min_{v \in S_h} \left(|u - v|_{W^1_\infty(\Omega_0)} + H^{-1} \|u - v\|_{L_\infty(\Omega_0)} \right) \\ &\quad + C H^{-1-s-2/q} \|u - u_h\|_{W_q^{-s}(\Omega_0)}.\end{aligned}$$

The corresponding result for the error in function values for $u - u_h$ is also found in [15].

Lemma 2.2. *Let u and u_h satisfy (2.1). Then for each $s \geq 0$ and $1 \leq q \leq \infty$ there exists a constant C such that*

$$\|u - u_h\|_{L_\infty(\Omega_1)} \leq C \left(\ln \frac{H}{h} \right)^{\bar{n}} \min_{v \in S_h} \|u - v\|_{L_\infty(\Omega_0)} + C H^{-s-2/q} \|u - u_h\|_{W_q^{-s}(\Omega_0)}.$$

Here $\bar{n} = 1$ if $n = 1$, $\bar{n} = 0$ otherwise.

Let Q be the $(n+1)^{th}$ order Taylor expansion of u at $\mathbf{x}^0$. Then

$$\|u - Q\|_{W^s_\infty(\Omega_0)} \leq C H^{n+2-s}, \quad \text{for} \quad 0 \leq s \leq n+2. \tag{2.4}$$

Interpolate it into $S_h(\Omega_0)$ to form $I_h Q$. Then set $\rho = Q - I_h Q$. The key observation in [2] is that ρ is $2h$-periodic. Let $S_h^\pi \left(c(\mathbf{x}^0, h) \right)$ denote the $2h$-periodic functions in $S_h \left(c(\mathbf{x}^0, h) \right)$, and define $PP(\rho) \in S_h^\pi \left(c(\mathbf{x}^0, h) \right)$ by

$$\int_{c(\mathbf{x}^0, h)} (\rho - PP(\rho)) = 0; \quad D_{c(\mathbf{x}^0, h)}(\rho - PP(\rho), v) = 0, \ \forall v \in S_h^\pi \left(c(\mathbf{x}^0, h) \right). \tag{2.5}$$

Denote $H^{1,\pi}(\Omega_0)$ the $2h$-periodic functions in $H^1(\Omega_0)$. Then from [2, 17], $\rho \in H^{1,\pi}(\Omega_0)$. The following lemma is also found in [2, 17].

Lemma 2.3. *For all $\varrho \in H^{1,\pi}(\Omega_0)$, we have*

$$D(\varrho - PP(\varrho), v) = 0, \quad \forall v \in S_h^{comp}(\Omega_0).$$

Now put $\psi = \rho - PP(\rho)$, by Lemma 2.1, we have [2, 17]

Theorem 2.1.

$$\frac{\partial}{\partial x_i}(u - u_h)(\mathbf{x}) = \frac{\partial \psi}{\partial x_i}(\mathbf{x}) + R_i(\mathbf{x}), \quad i = 1, 2, \quad \mathbf{x} \in \Omega_1,$$

where

$$\|R_i\|_{L_\infty(\Omega_1)} \leq C \left(h^{n+\delta} + h^{n+1-L-\delta} \right),$$

provided $L + \delta < 1$.

Remark 2.1. Theorem 2.1 states that the major part of the finite element approximation error in the derivatives can be measured by $\frac{\partial \psi}{\partial x_i}(\mathbf{x})$, since the remainder is of an order $\min(\delta, 1 - L - \delta)$ higher than the global convergence rate. □

In this work, we establish an analogue of Theorem 2.1 for the error in function values.

Theorem 2.2.

$$(u-u_h)(\mathbf{x}) = \psi(\mathbf{x}) + R_u(\mathbf{x}), \quad \mathbf{x} \in \Omega_1,$$

where

$$\|R_u\|_{L_\infty(\Omega_1)} \leq C\left(\ln \tfrac{1}{h}\right)^{\bar{n}} h^{n+1+\delta} + Ch^{n+2-\Lambda-\delta},$$

provided $\Lambda + \delta < 1$.

Proof. Let N_hQ be the Neumann projection of Q into $S_h(\Omega_0)$, i.e.

$$\int_{\Omega_0} (Q - N_hQ) = 0; \quad D(Q - N_hQ, v) = 0, \ \forall v \in S_h(\Omega_0). \tag{2.6}$$

Then we can write

$$u - u_h = (Q - N_hQ) + [(u - Q) - (u_h - N_hQ)]. \tag{2.7}$$

We denote $R_Q = [(u - Q) - (u_h - N_hQ)]$.

From (2.1) and (2.6) we get

$$D(R_Q, v) = 0, \quad \forall v \in S_h^{comp}(\Omega_0).$$

By Lemma 2.2,

$$\|R_Q\|_{L_\infty(\Omega_1)} \leq C\left(\ln \frac{1}{h}\right)^{\bar{n}} \min_{v \in S_h} \|(u - Q) - v\|_{L_\infty(\Omega_0)} + CH^{-1}\|R_Q\|_{W_\infty^{-1}(\Omega_0)}. \tag{2.8}$$

Letting v be the interpolation of $u - Q$ into $S_h(\Omega_0)$. From assumption (2.4),

$$\|(u - Q) - v\|_{L_\infty(\Omega_0)} \leq Ch^{n+1}\|u - Q\|_{W_\infty^{n+1}(\Omega_0)} \leq Ch^{n+1}H. \tag{2.9}$$

By assumption (2.3)

$$\|R_Q\|_{W_\infty^{-1}(\Omega_0)} \leq \|u - u_h\|_{W_\infty^{-1}(\Omega_0)} + \|Q - N_hQ\|_{W_\infty^{-1}(\Omega_0)} \leq Ch^{n+2-\Lambda}. \tag{2.10}$$

Hence (2.8) – (2.10) give

$$\|R_Q\|_{L_\infty(\Omega_1)} \leq C\left(\ln \frac{1}{h}\right)^{\bar{n}} h^{n+1}H + CH^{-1}h^{n+2-\Lambda}. \tag{2.11}$$

Recall that $\rho = Q - I_hQ$ and $\psi = \rho - PP(\rho)$. Rewrite

$$Q - N_hQ = \psi + [Q - N_hQ - \psi].$$

Notice that

$$Q - N_hQ - \psi = I_hQ + PP(\rho) - N_hQ \in S_h(\Omega_0). \tag{2.12}$$

From Lemma 2.3 and (2.6), we get

$$D(Q - N_hQ - \psi, v) = 0, \quad \forall v \in S_h^{comp}(\Omega_0).$$

From Lemma 2.2 and (2.12),

$$\|Q - N_h Q - \psi\|_{L_\infty(\Omega_1)} \leq CH^{-1}\|Q - N_h Q - \psi\|_{W_\infty^{-1}(\Omega_0)}. \tag{2.13}$$

By assumption (2.3)

$$\|Q - N_h Q\|_{W_\infty^{-1}(\Omega_0)} \leq Ch^{n+2-\Lambda}. \tag{2.14}$$

By a duality argument,

$$\|\psi\|_{W_\infty^{-1}(\Omega_0)} \leq \|\rho\|_{W_\infty^{-1}(\Omega_0)} \leq Ch^{n+2}\|Q\|_{W_\infty^{n+1}(\Omega_0)} \leq Ch^{n+2-\Lambda}. \tag{2.15}$$

Therefore, from (2.13) – (2.15),

$$\|Q - N_h Q - \psi\|_{L_\infty(\Omega_1)} \leq CH^{-1}h^{n+2-\Lambda}. \tag{2.16}$$

Finally, we set $R_u = (u - u_h) - \psi$. From (2.7), (2.11), and (2.16), we get

$$\begin{aligned} \|R_u\|_{L_\infty(\Omega_1)} &\leq C\left(\ln\tfrac{1}{h}\right)^{\bar{n}} h^{n+1}H + CH^{-1}h^{n+2-\Lambda} \\ &\leq C\left(\ln\tfrac{1}{h}\right)^{\bar{n}} h^{n+1+\delta} + Ch^{n+2-\Lambda-\delta}, \end{aligned} \tag{2.17}$$

and the theorem follows. □

Remark 2.2. Theorem 2.2 indicates that ψ gives the main part of the error in function values. The convergence rate of the remainder is of an order $\min(\delta, 1-\Lambda-\delta)$ higher than the global rate. □

Remark 2.3. By Remarks 2.1, 2.2, the task of finding superconvergent points can be narrowed down to a master cell, or equivalently to the reference cell $\hat{K} = [-1,1]^2$. And the superconvergent points of derivatives and function values are those points $\mathbf{x}$ where $\frac{\partial\psi}{\partial x_i}(\mathbf{x}) = 0$ and $\psi(\mathbf{x}) = 0$, respectively. Thus, the task of identifying superconvergent points is equivalent to finding the critical points of some periodic polynomials ψ of degree $n+1$ on the reference cell $\hat{K}$ such that $\psi \notin V_n(\hat{K})$, and

$$\int_{\hat{K}} \psi = 0; \quad \int_{\hat{K}} \nabla\psi \cdot \nabla v = 0, \ \forall v \in V_n^\pi(\hat{K}),$$

where $V_n(\hat{K})$ and $V_n^\pi(\hat{K})$ are the images of $S_h\left(c(\mathbf{x}^0, h)\right)$ and $S_h^\pi\left(c(\mathbf{x}^0, h)\right)$, respectively. In another word, $V_n(\hat{K})$ and $V_n^\pi(\hat{K})$ are the finite element local space and the *periodic* finite element local space on the reference cell $\hat{K}$, respectively. □

3. SUPERCONVERGENT POINTS FOR PERIODIC MESHES OF TRIANGLES

For periodic uniform triangular local mesh, we consider four patterns: *Regular* pattern, *Chevron* pattern, *Union Jack* pattern, and *Criss-Cross* pattern (see FIGURE 1). These patterns were discussed by Babuška, *et al.* in [2].

Clearly, a mesh in any one of these four patterns is a local translation invariant. Hence, the assumption (b) in Section 2 is satisfied. In addition, we require the assumption (c) from now on.

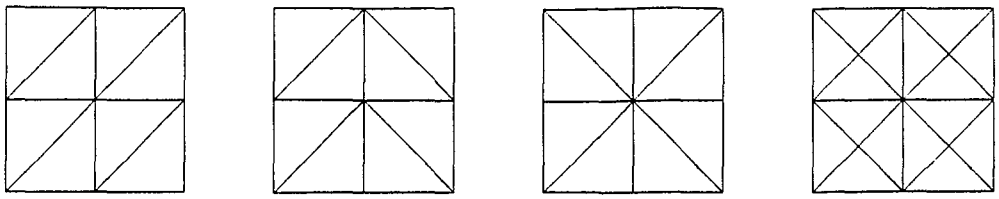

Regular Pattern Chevron Pattern Union Jack Pattern Criss-Cross Pattern

Figure 1: Periodic Meshes of Triangles

In the following, we study the superconvergent points of function values and derivatives for the Poisson and Laplace equations. Their solutions are approximated by finite element spaces with polynomials and harmonic polynomials, respectively.

For each pattern, the finite element local space $V_n(\hat{K})$ is the space of *continuous piecewise* polynomials on $\hat{K}$; the *periodic* finite element local space $V_n^\pi(\hat{K})$ is the space of *periodic continuous piecewise* polynomials on $\hat{K}$. $V_n(\hat{K})$ and $V_n^\pi(\hat{K})$ are both subspaces of $C^0(\hat{K})$. Structures of $V_n(\hat{K})$ and $V_n^\pi(\hat{K})$ associated with different mesh patterns are different.

We shall show the study of the regular pattern in details, and present only the main results for the other three patterns.

For finite elements with various mesh patterns and degrees, we locate the superconvergent points for solutions of (i) the Poisson equation; and (ii) the Laplace equation. Based on results in Section 2, we set u to be Q for (i) the class of general polynomials $x^{n+1}, x^n y, \ldots, y^{n+1}$ (for the Poisson equation); and (ii) the class of harmonic polynomials $Re(z^{n+1})$ and $Im(z^{n+1})$ (for the Laplace equation).

In the context, $\square^{Rg}$, $\square^{Ch}$, $\square^{UJ}$, and $\square^{CC}$ will be used to denote the object $\square$ defined in the regular, Chevron, Union Jack, and the Criss-Cross patterns, respectively.

3.1. Regular Pattern

3.1.1. Preliminaries and Theorems

Set the reference cell $\hat{K} = [-1, 1]^2$. Partition $\hat{K}$ into two triangular elements and denote them as $\hat{T}_1 = \{(x, y) \in \hat{K} | x \geq y\}$, $\hat{T}_2 = \{(x, y) \in \hat{K} | x \leq y\}$ (see FIGURE 2). In the following, we denote $\hat{T}_i$ the i^{th} element, n_i the i^{th} node, and l_{ij} the side connecting n_i and n_j.

Define $P_n^w(\hat{K})$ the space of *continuous piecewise* polynomials of degree not greater than n on $\hat{K}$. That is, for any $f \in P_n^w(\hat{K})$, f is continuous on $\hat{K}$; $f|_{\hat{T}_1}$, $f|_{\hat{T}_2}$ are polynomials of degree ($\leq n$). Let $PP_n^w(\hat{K})$ be the space of *periodic continuous piecewise* polynomials of degree not greater than n on $\hat{K}$. In other words, if $f \in PP_n^w(\hat{K})$, then $f \in P_n^w(\hat{K})$, and $f(x, 1) = f(x, -1)$, $f(1, y) = f(-1, y)$. Denote $P_n(\hat{K})$ the space of polynomials of degree not greater than n on $\hat{K}$.

From the definitions, we conclude that, in general, $P_n(\hat{K}) \subset P_n^w(\hat{K})$ and $PP_n^w(\hat{K}) \subset P_n^w(\hat{K})$. Moreover, the finite element local space $V_n(\hat{K})$ is $P_n^w(\hat{K})$, and the *periodic* finite element local space $V_n^\pi(\hat{K})$ is $PP_n^w(\hat{K})$. We shall use these two sets of notations alternatively. However, V_n and V_n^π are preferred when we consider finite element approximation.

Define $\Phi_{n+1}(\hat{K})$ the subspace of $PP_{n+1}^w(\hat{K})$ that consists of functions ψ, which can be

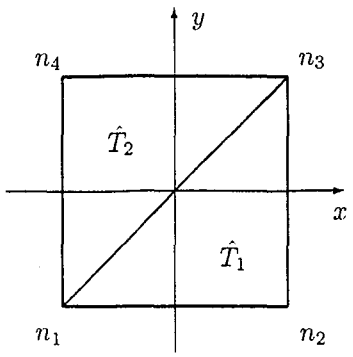

Figure 2: Partition of $\hat{K}$ for the Regular Pattern

decomposed into $P_{n+1}(\hat{K})$ and $P_n^w(\hat{K})$, such that

$$\int_{\hat{K}} \psi = 0; \quad \int_{\hat{K}} \nabla\psi \cdot \nabla v = 0, \ \forall v \in PP_n^w(\hat{K}). \tag{3.1}$$

In other words, for any $\psi \in \Phi_{n+1}(\hat{K})$, we have $\psi = \chi + r$ satisfying (3.1), where $\chi \in P_{n+1}(\hat{K})$ and $r \in P_n^w(\hat{K})$.

Lemma 3.1. $\dim\Phi_{n+1}(\hat{K}) = n + 2$.

Proof. Suppose $\psi_i \in \Phi_{n+1}(\hat{K})$ with $\psi_i = \chi + r_i$, where $\chi \in P_{n+1}(\hat{K})$ and $r_i \in P_n^w(\hat{K})$, $i = 1, 2$. Set $\delta = \psi_1 - \psi_2$. Clearly, δ is periodic. Also $\delta = r_1 - r_2$, which implies $\delta \in P_n^w(\hat{K})$. Thus, $\delta \in PP_n^w(\hat{K})$. From (3.1), we conclude that

$$\int_{\hat{K}} \delta = 0; \quad \int_{\hat{K}} \nabla\delta \cdot \nabla v = 0, \ \forall v \in PP_n^w(\hat{K}).$$

But this happens only when $\delta \equiv 0$. Therefore, the dimension of $\Phi_{n+1}(\hat{K})$ is the same as the dimension of the space of monomials of degree $n + 1$, which is $n + 2$. □

From Theorems 2.1, 2.2, and Remark 2.3, we get

Theorem 3.1. *(i) Function value superconvergent points of $V_n(\hat{K})$ for the Poisson equation are the intersections of the contours*

$$\{\psi = 0 \mid \psi \in \Phi_{n+1}(\hat{K})\}.$$

(ii) Derivative superconvergent points of $V_n(\hat{K})$ along the x-direction for the Poisson equation are the intersections of the contours

$$\{\frac{\partial\psi}{\partial x} = 0 \mid \psi \in \Phi_{n+1}(\hat{K})\}.$$

Similar result holds on the y-direction.

Applying Theorems 2.1 and 2.2 to the case of harmonic functions (solutions of the Laplace equation) yields the following theorem.

Theorem 3.2. *(i) Function value superconvergent points of $V_n(\hat{K})$ for the Laplace equation are the intersections of the contours*

$$\psi_{n+1}^{Re} = 0 \quad \textit{and} \quad \psi_{n+1}^{Im} = 0,$$

with

$$\psi_{n+1}^{Re} = Re(z^{n+1}) - r_n, \quad \psi_{n+1}^{Im} = Im(z^{n+1}) - s_n,$$

where

$$\psi_{n+1}^{Re},\ \psi_{n+1}^{Im} \in \Phi_{n+1}(\hat{K}); \quad r_n, s_n \in V_n(\hat{K}); \quad z = x + iy.$$

(ii) Derivative superconvergent points of $V_n(\hat{K})$ along the x-direction for the Laplace equation are the intersections of the contours

$$\frac{\partial \psi_{n+1}^{Re}}{\partial x} = 0 \quad \textit{and} \quad \frac{\partial \psi_{n+1}^{Im}}{\partial x} = 0.$$

Similar result holds on the y-direction.

Proof. Let u be any harmonic function. The $(n+1)^{th}$ order Taylor expansion of u at the center of $\hat{K}$ is of the form $\alpha Re(z^{n+1}) + \beta Im(z^{n+1}) + t_n$, where $\alpha, \beta \in \mathbb{R}$ and $t_n \in P_n(\hat{K})$. Therefore, the results follow from Theorems 2.1 and 2.2. □

Remark 3.1. Theorems 3.1 and 3.2 indicate that to locate superconvergent points of function values and derivatives for the Poisson and Laplace equations, we need to specify spaces $\Phi_{n+1}(\hat{K})$. We next determine a basis for each $\Phi_{n+1}(\hat{K})$ via an orthogonal decomposition of $PP_{n+1}^w(\hat{K})$. □

3.1.2. Orthogonal Decomposition of $PP_n^w(\hat{K})$ and Construction of $\Phi_{n+1}(\hat{K})$

In current work, a set of hierarchic basis functions are used for $V_n(\hat{K})$. The basis functions can be organized into three categories: nodal shape functions, side modes and internal modes (see [16, Chapter 6]). There are 4 nodal shape functions, which are denoted as ν_i, $i = 1, \ldots, 4$.

$$\begin{aligned} \nu_1 &= \begin{cases} \frac{1}{2}(1-x) & \text{in } \hat{T}_1, \\ \frac{1}{2}(1-y) & \text{in } \hat{T}_2; \end{cases} \quad \nu_2 = \begin{cases} \frac{1}{2}(x-y) & \text{in } \hat{T}_1, \\ 0 & \text{in } \hat{T}_2; \end{cases} \\ \nu_3 &= \begin{cases} \frac{1}{2}(1+y) & \text{in } \hat{T}_1, \\ \frac{1}{2}(1+x) & \text{in } \hat{T}_2; \end{cases} \quad \nu_4 = \begin{cases} 0 & \text{in } \hat{T}_1, \\ \frac{1}{2}(y-x) & \text{in } \hat{T}_2. \end{cases} \end{aligned} \tag{3.2}$$

Clearly, we have

$$\nu_1(-x,-y) = \nu_3(x,y), \quad \text{and} \quad \nu_2(-x,-y) = \nu_4(x,y). \tag{3.3}$$

Side modes and internal modes are constructed from the nodal shape functions in the following means. Let p_k be the Legendre polynomial of degree k on $[-1,1]$. Define

$$\begin{aligned} \phi_0(x) &= 1, \quad \phi_1(x) = x, \\ \phi_k(x) &= \int_{-1}^{x} p_{k-1}(t)dt, \quad k = 2, 3, \ldots \end{aligned} \tag{3.4}$$

For $k \geq 2$, since $\varphi_k(x)$ are polynomials which vanish at $x = \pm 1$, the term $1 - x^2$ can be factored out. We define $\varphi_k(x)$ so that

$$\phi_k(x) = \frac{1}{4}(1 - x^2)\varphi_{k-2}(x), \quad k = 2, 3, \ldots \tag{3.5}$$

The subscripts of ϕ_k and φ_k indicate the orders (degrees) of the polynomials.

Denote ς_k^{ij} the k^{th} order side mode along the side l_{ij}. Define the side modes associated with side l_{12} as

$$\varsigma_k^{12} = \nu_1\nu_2\ \varphi_{k-2}(\nu_2 - \nu_1), \quad k = 2, \ldots, n. \tag{3.6}$$

The other side modes are defined analogously. There are $n - 1$ side modes on each side.

Denote $\iota_{k,j}^i$ the j^{th} internal mode on $\hat{T}_i$ of order k. In the first element $\hat{T}_1$, the internal modes are defined as

$$\iota_{k,j}^1 = \nu_1\nu_2\nu_3\ x^{j-1}y^{k-j-2}, \quad k = 3, \ldots, n;\ j = 1, \ldots, k-2. \tag{3.7}$$

The definition of the internal modes in $\hat{T}_2$ is similar. There are $(n-1)(n-2)/2$ internal modes in each element.

Notice that $V_n(\hat{K}) = P_n^w(\hat{K})$, the dimension of $P_n^w(\hat{K})$ can be decided from that of $V_n(\hat{K})$. Sum up the numbers of nodal shape functions, side modes and internal modes, we have

$$\dim\ P_n^w(\hat{K}) = 4 + 5(n-1) + 2\frac{(n-1)(n-2)}{2} = (n+1)^2. \tag{3.8}$$

A basis for $PP_n^w(\hat{K})$ may be constructed from the hierarchic basis functions of $P_n^w(\hat{K})$. In fact, the sum of the four nodal shape functions $\nu_1 + \nu_2 + \nu_3 + \nu_4$ is a periodic basis function. The sums of the same order side modes along the opposite boundary sides are periodic basis functions. The side modes along the interior sides and all of the internal modes are automatically periodic. To simplify notations, in the context, we denote $\varsigma_k^d = \varsigma_k^{13}$, $\varsigma_k^h = \varsigma_k^{12} + \varsigma_k^{43}$, $\varsigma_k^v = \varsigma_k^{23} + \varsigma_k^{14}$, which represent the k^{th} order diagonal, horizontal, and vertical periodic side modes. Also denote $\iota_{k,j}^{\pm} = \iota_{k,j}^1 \pm \iota_{k,j}^2$, which are referred as k^{th} order internal modes of *plus/minus* type.

An example of the construction of $PP_n^w(\hat{K})$ is given for case $n = 3$ (see FIGURE 3).

$$\begin{array}{c} \nu = \nu_1 + \nu_2 + \nu_3 + \nu_4 \equiv 1, \\ \varsigma_2^h = \varsigma_2^{12} + \varsigma_2^{43}, \quad \varsigma_2^v = \varsigma_2^{23} + \varsigma_2^{14}, \quad \varsigma_2^d = \varsigma_2^{13}, \\ \varsigma_3^h = \varsigma_3^{12} + \varsigma_3^{43}, \quad \varsigma_3^v = \varsigma_3^{23} + \varsigma_3^{14}, \quad \varsigma_3^d = \varsigma_3^{13}, \\ \iota_{3,1}^1, \quad \iota_{3,1}^2. \end{array} \tag{3.9}$$

The dimension of $PP_n^w(\hat{K})$ can be determined by deleting 3 nodal freedoms and $2(n-1)$ side mode freedoms from $\dim P_n^w(\hat{K})$. Hence,

$$\dim\ PP_n^w(\hat{K}) = \dim\ P_n^w(\hat{K}) - 3 - 2(n-1) = n^2. \tag{3.10}$$

Lemma 3.2. *(i)* $\phi_{k+1}(-x) = (-1)^{k+1}\phi_{k+1}(x)$ *for* $k = 1, 2, \ldots$;
(ii) $\varphi_k(-x) = (-1)^k\varphi_k(x)$ *for* $k = 0, 1, \ldots$;

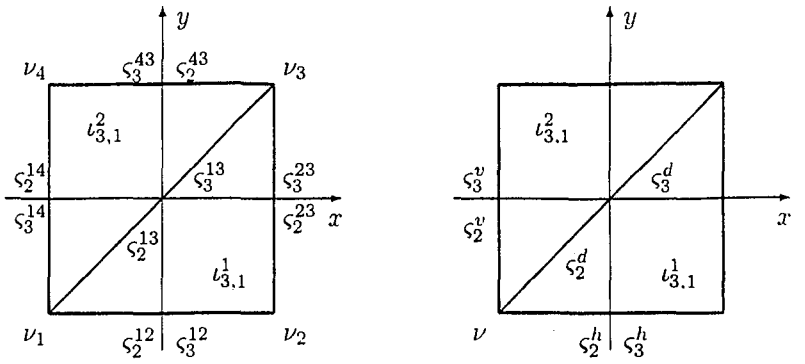

(*a*) Hierarchic basis for $P_3^w(\hat{K})$ (*b*) Periodic basis for $PP_3^w(\hat{K})$

Figure 3: Basis functions for $P_3^w(\hat{K})$ and $PP_3^w(\hat{K})$.

(*iii*) $\varsigma_k^t(-x,-y) = (-1)^k \varsigma_k^t(x,y)$ *for* $t = h, v, d$, *and* $k = 2, \ldots, n$;
(*iv*) $\iota_{k,j}^1(-x,-y) = (-1)^{k-1} \iota_{k,j}^2(x,y)$ *for* $k = 3, \ldots, n$, *and* $j = 1, \ldots, k-2$.
Moreover, $\iota_{k,j}^+(-x,-y) = (-1)^{k-1} \iota_{k,j}^+(x,y)$, *and* $\iota_{k,j}^-(-x,-y) = (-1)^k \iota_{k,j}^-(x,y)$.

Proof. (*i*) Since $\phi_{k+1}(1) = 0$ and $p_k(-x) = (-1)^k p_k(x)$ for any k, the assertion follows from definition (3.4).
(*ii*) By (3.5) and result of part (*i*), the desired result follows.
(*iii*) This is a consequence of definition (3.6), properties (3.3), and result of part (*ii*).
(*iv*) Definition (3.7) and properties (3.3) give (*iv*). □

Lemma 3.2 states that the periodic basis functions are either even or odd.

Further, we consider the orthogonal decomposition of $PP_n^w(\hat{K})$ under the Laplace operator. Towards this end, we define

$$\Psi_{n+1}(\hat{K}) = \{u \in PP_{n+1}^w(\hat{K}) \mid \int_{\hat{T}_1 \cup \hat{T}_2} \nabla u \cdot \nabla v = 0, \ \forall v \in PP_n^w(\hat{K})\}. \tag{3.11}$$

Compare (3.11) with (3.1). Clearly, $\Phi_{n+1}(\hat{K}) \subset \Psi_{n+1}(\hat{K})$, in general.

By the Gram-Schmidt process, we can decompose $PP_n^w(\hat{K})$ into

$$PP_n^w(\hat{K}) = PP_0^w(\hat{K}) \oplus \Psi_2(\hat{K}) \oplus \cdots \oplus \Psi_{n-1}(\hat{K}) \oplus \Psi_n(\hat{K}). \tag{3.12}$$

Note that $PP_0^w(\hat{K}) = \text{Span}\{1\}$ and $\Psi_1(\hat{K}) = \{0\}$. The dimension of $\Psi_{n+1}(\hat{K})$ can be determined as

$$\dim \Psi_{n+1}(\hat{K}) = \dim PP_{n+1}^w(\hat{K}) - \dim PP_n^w(\hat{K}) = 2n+1, \quad n = 1, 2, 3, \ldots \tag{3.13}$$

The first two spaces of $\Psi_{n+1}(\hat{K})$ $(n = 1, 2)$ can be expressed as

$$\Psi_2(\hat{K}) = \text{Span}\left\{\phi_2(x), \ \varsigma_2^d, \ \phi_2(y)\right\};$$

$$\Psi_3(\hat{K}) = \text{Span}\left\{\phi_3(x), \ \pm\varsigma_3^d + 18\iota_{3,1}^1 + 2\iota_{3,1}^2 + \varsigma_2^h + \varsigma_2^v + \varsigma_2^d, \right.$$
$$\left. 16\iota_{3,1}^1 + 4\iota_{3,1}^2 + \varsigma_2^h + \varsigma_2^v + \varsigma_2^d, \ \phi_3(y)\right\}.$$

The space $\Phi_{n+1}(\hat{K})$ can be constructed from $\Psi_{n+1}(\hat{K})$. For instance, for $n = 1, 2$, we get

$$\Phi_2(\hat{K}) = \text{Span}\left\{\phi_2(x) + \tfrac{1}{3},\ \varsigma_2^d + \tfrac{1}{6},\ \phi_2(y) + \tfrac{1}{3}\right\};$$

$$\Phi_3(\hat{K}) = \text{Span}\left\{\phi_3(x),\ \phi_2(x)y + \varsigma_2^{12} - \varsigma_2^{43},\ x\phi_2(y) - \varsigma_2^{23} + \varsigma_2^{14},\ \phi_3(y)\right\}.$$

By the Gram-Schmidt process, we can obtain more spaces of $\Psi_{n+1}(\hat{K})$, and thus more spaces of $\Phi_{n+1}(\hat{K})$. Here, we give two more $\Phi_{n+1}(\hat{K})$ (for $n = 3, 4$) without the associated $\Psi_{n+1}(\hat{K})$.

$$\begin{aligned}\Phi_4(\hat{K}) = \text{Span}\big\{&\phi_4(x) + r_3^0,\quad \phi_3(x)y + \varsigma_3^{12} - \varsigma_3^{43} + r_3^1,\quad \phi_2(x)\phi_2(y) + r_3^2,\\ &x\phi_3(y) - \varsigma_3^{23} + \varsigma_3^{14} + r_3^3,\quad \phi_4(y) + r_3^4\big\},\end{aligned}$$

where

$$\begin{aligned} r_3^0 = r_3^4 &= \tfrac{1}{14} + \tfrac{3}{14}(\varsigma_2^h + \varsigma_2^v) + \tfrac{3}{14}\varsigma_2^d + \tfrac{15}{7}\iota_{3,1}^+,\\ r_3^1 = r_3^3 &= \tfrac{1}{21} + \tfrac{1}{7}(\varsigma_2^h + \varsigma_2^v) - \tfrac{2}{35}\varsigma_2^d - \tfrac{4}{7}\iota_{3,1}^+,\\ r_3^2 &= \tfrac{2}{63} + \tfrac{2}{21}(\varsigma_2^h + \varsigma_2^v) + \tfrac{52}{105}\varsigma_2^d - \tfrac{12}{7}\iota_{3,1}^+;\end{aligned}$$

$$\begin{aligned}\Phi_5(\hat{K}) = \text{Span}\big\{&\phi_5(x) + r_4^0,\quad \phi_4(x)y + \varsigma_4^{12} - \varsigma_4^{43} + r_4^1,\quad \phi_3(x)\phi_2(y) + r_4^2,\\ &\phi_2(x)\phi_3(y) + r_4^3,\quad x\phi_4(y) - \varsigma_4^{23} + \varsigma_4^{14} + r_4^4,\quad \phi_5(y) + r_4^5\big\},\end{aligned}$$

where

$$\begin{aligned} r_4^0 &= \tfrac{5}{24}\varsigma_3^h + \tfrac{5}{72}\varsigma_3^v - \tfrac{5}{36}\varsigma_3^d - \tfrac{35}{36}\iota_{3,1}^- + \tfrac{245}{72}\iota_{4,1}^+ + \tfrac{35}{72}\iota_{4,2}^+,\\ r_4^1 &= \tfrac{55}{504}\varsigma_3^h + \tfrac{25}{504}\varsigma_3^v + \tfrac{13}{63}\varsigma_3^d + \tfrac{59}{42}\iota_{3,1}^- - \tfrac{235}{72}\iota_{4,1}^+ + \tfrac{125}{72}\iota_{4,2}^+,\\ r_4^2 &= \tfrac{5}{126}\varsigma_3^h + \tfrac{1}{42}\varsigma_3^v - \tfrac{20}{36}\varsigma_3^d - \tfrac{52}{63}\iota_{3,1}^- - \tfrac{43}{18}\iota_{4,1}^+ + \tfrac{5}{18}\iota_{4,2}^+,\\ r_4^3 &= \tfrac{1}{42}\varsigma_3^h + \tfrac{5}{126}\varsigma_3^v - \tfrac{20}{36}\varsigma_3^d + \tfrac{52}{63}\iota_{3,1}^- + \tfrac{5}{18}\iota_{4,1}^+ - \tfrac{43}{18}\iota_{4,2}^+,\\ r_4^4 &= \tfrac{25}{504}\varsigma_3^h + \tfrac{55}{504}\varsigma_3^v + \tfrac{13}{63}\varsigma_3^d - \tfrac{59}{42}\iota_{3,1}^- + \tfrac{125}{72}\iota_{4,1}^+ - \tfrac{235}{72}\iota_{4,2}^+,\\ r_4^5 &= \tfrac{5}{72}\varsigma_3^h + \tfrac{5}{24}\varsigma_3^v - \tfrac{5}{36}\varsigma_3^d + \tfrac{35}{36}\iota_{3,1}^- + \tfrac{35}{72}\iota_{4,1}^+ + \tfrac{245}{72}\iota_{4,2}^+.\end{aligned}$$

For information of cases $n = 5, \ldots, 8$, the reader is referred to [13].

We shall study the structures of functions in $\Phi_{n+1}(\hat{K})$ for general n (> 2). By the definition of $\Phi_{n+1}(\hat{K})$ in (3.1), every function in $\Phi_{n+1}(\hat{K})$ can be decomposed into a part in $P_{n+1}(\hat{K})$ and a part in $P_n^w(\hat{K})$. As shown in Lemma 3.1, the dominating part in $P_{n+1}(\hat{K})$ has a basis $\{\phi_{n+1-j}(x)\phi_j(y)\}_{j=0}^{n+1}$. The remaining term in $P_n^w(\hat{K})$ insures that the function lies in $\Phi_{n+1}(\hat{K})$. We need to determine the patterns of these remaining terms.

From the above description, $\Phi_{n+1}(\hat{K})$ can be constructed from periodic basis functions. We know that $\phi_{n+1-j}(x)\phi_j(y)$ are in $PP_{n+1}^w(\hat{K})$, except for $j = 1$ and n. We shall modify $\phi_n(x)y$ and $x\phi_n(y)$. Since the restriction of ς_n^{12} on l_{12} is $\phi_n(x)$; and similar situation happens on the other boundary sides of $\hat{K}$, we conclude that $\phi_n(x)y + \varsigma_n^{12} - \varsigma_n^{43}$ and $x\phi_n(y) - \varsigma_n^{23} + \varsigma_n^{14}$ vanish on the boundary of $\hat{K}$, and hence are in $PP_{n+1}^w(\hat{K})$.

After getting these modified $(n+1)^{th}$ order periodic polynomials, we denote all the remaining terms as r_n^j. Since $\Phi_{n+1}(\hat{K}) \subset PP_{n+1}^w(\hat{K})$, it is clear that $r_n^j \in PP_n^w(\hat{K})$. Then we have the following lemma.

Lemma 3.3. *For each* $\psi \in \Phi_{n+1}(\hat{K})$, $\psi(-x,-y) = (-1)^{n+1}\psi(x,y)$. *Moreover, we have* $\nabla\psi(-x,-y) = (-1)^n\nabla\psi(x,y)$.

Proof. It is straightforward to check that the lemma holds for $n = 1, 2$. We assume $n > 2$ in the following. It is sufficient to show the symmetric properties hold for basis functions.

For $j = 0, \ldots, n+1$, $j \neq 1, n$, the j^{th} basis function in $\Phi_{n+1}(\hat{K})$ is written as

$$B_{n+1}^j = \varphi_{n+1-j}(x)\phi_j(y) + r_n^j.$$

By definition (3.1), for all $v \in PP_n^w(\hat{K})$,

$$\int_{\hat{K}} \nabla B_{n+1}^j \cdot \nabla v = \int_{\hat{K}} \nabla(\phi_{n+1-j}(x)\phi_j(y)) \cdot \nabla v + \int_{\hat{K}} \nabla r_n^j \cdot \nabla v = 0.$$

From Lemma 3.2, we have

$$\nabla(\phi_{n+1-j}(-x)\phi_j(-y)) = (-1)^n\nabla(\phi_{n+1-j}(x)\phi_j(y)).$$

If n is even, pick v even. Then ∇v is odd, and $\nabla(\phi_{n+1-j}(x)\phi_j(y)) \cdot \nabla v$ is odd. We have

$$\int_{\hat{K}} \nabla(\phi_{n+1-j}(x)\phi_j(y)) \cdot \nabla v = 0, \quad \text{and hence} \quad \int_{\hat{K}} \nabla r_n^j \cdot \nabla v = 0.$$

Note that r_n^j is in $PP_n^w(\hat{K})$, which has basis functions either even or odd. Let v run through all even basis functions, we conclude that r_n^j is odd, just as $\phi_{n+1-j}(-x)\phi_j(-y)$. Therefore, B_{n+1}^j is odd, as desired. Similarly, if n is odd, we shall conclude that B_{n+1}^j is even.

For $j = 1$ and n, the desired results shall follow if $\varsigma_n^{12} - \varsigma_n^{43}$ and $-\varsigma_n^{23} + \varsigma_n^{14}$ have proper symmetry properties. Namely, if n is even, both of them are odd; if n is odd, both of them are even. These follow from (3.3), (3.6), and Lemma 3.2. □

Remark 3.2. Lemma 3.3 reveals that, to locate superconvergent points in $\hat{K}$, we need to consider only the situations in $\hat{T}_1$. The superconvergent points in $\hat{T}_2$ are symmetric to those in $\hat{T}_1$ about the origin. □

Lemma 3.2 also induces general expressions of basis functions in $\Phi_{n+1}(\hat{K})$.

Theorem 3.3. *For all* $n > 2$, *we have*

$$\begin{aligned}\Phi_{n+1}(\hat{K}) = \ & \text{Span}\{\phi_{n+1}(x) + r_n^0, \quad \phi_n(x)y + \varsigma_n^{12} - \varsigma_n^{43} + r_n^1, \\ & \phi_{n+1-j}(x)\phi_j(y) + r_n^j \quad (j = 2, \ldots, n-1), \\ & x\phi_n(y) - \varsigma_n^{23} + \varsigma_n^{14} + r_n^n, \quad \phi_{n+1}(y) + r_n^{n+1}\},\end{aligned}$$

where r_n^j*s satisfy the following property:*
(i) For even order r_n^j*s, only odd order side modes, odd order internal modes of minus type, and even order internal modes of plus type are involved in the expressions;*
(ii) For odd order r_n^j*s, only even order side modes, odd order internal modes of plus type, and even order internal modes of minus type are involved in the expressions.*

Proof. Note that any function in $\Phi_{n+1}(\hat{K})$ is expressed in terms of periodic side modes and internal modes. This is a direct result from Lemmas 3.2 and 3.3. □

Remark 3.3. As we have seen above, the expressions of basis functions in $\Phi_{n+1}(\hat{K})$ obtained from the orthogonal decomposition reveal the structure of them (in terms of *periodic* basis

functions). This may provide us an analytical way to find superconvergent points. However, this approach is quite complicated, especially when n is large.

In fact, if we are interested only in the expressions (not the structures) of the basis functions in $\Phi_{n+1}(\hat{K})$, then we can simplify the process by solving

$$\int_{\hat{K}} \nabla(u - I_h u - z) \cdot \nabla v = 0, \quad \forall v \in V_n^{\pi}(\hat{K}); \tag{3.14}$$

$$\int_{\hat{K}} (u - I_h u - z) = 0, \tag{3.15}$$

where u are monomials of degree $n+1$, $I_h u$ is an interpolation of u in $V_n(\hat{K})$, and z is a *periodic* finite element approximation of $u - I_h u$. Then $u - I_h u - z$ will serve as a periodic basis function in $\Phi_{n+1}(\hat{K})$ corresponding to u.

The approach works as the following. An interpolation $I_h u$ in $V_n(\hat{K})$ are determined from the conditions:

$$\text{(i)} \quad I_h u(\pm 1, \pm 1) = u(\pm 1, \pm 1); \tag{3.16}$$

$$\text{(ii)} \quad \int_l (u - I_h u) s^j ds = 0, \quad j = 0, 1, \cdots, n-2, \tag{3.17}$$

along each side l in $\hat{K}$; and

$$\text{(iii)} \quad \int_{\hat{T}} (u - I_h u) x^j y^k dx dy = 0, \quad j, k \geq 0, \ \ j + k = 0, 1, \cdots, n-3, \tag{3.18}$$

on each element $\hat{T}$ in $\hat{K}$.

After $I_h u$ is determined, the *periodic* finite element approximation z of $u - I_h u$ can be achieved by solving (3.14) and (3.15). Here, the *periodic* basis functions of $V_n^{\pi}(\hat{K})$ are described above.

For instance, consider the *periodic* basis function corresponding to $x^3 y$ in $\Phi_4(\hat{K})$. This is a case for $n = 3$ (see FIGURE 3). First interpolate $x^3 y$ in $V_3(\hat{K})$. The restriction of the interpolation $I_h(x^3 y)$ on $\hat{T}_i$ is a polynomial of degree (≤ 3); i.e.

$$I_h(x^3 y)|_{\hat{T}_i} = \sum_{0 \leq j+k \leq 3} c_{j,k}^i \, x^j y^k, \quad j, k \geq 0, \quad i = 1, 2. \tag{3.19}$$

Substituting $I_h(x^3 y)|_{\hat{T}_i}$ in conditions (3.16)–(3.18), we have a system of equations for $c_{j,k}^i$s on each $\hat{T}_i$. Use $\begin{pmatrix} f_1(x,y) \\ f_2(x,y) \end{pmatrix}$ to denote the piecewise polynomial $\begin{cases} f_1(x,y) & in \ \ \hat{T}_1, \\ f_2(x,y) & in \ \ \hat{T}_2. \end{cases}$ With help of a symbolic computation software (MAPLE), we can solve the systems and obtain

$$I_h(x^3 y) = \begin{pmatrix} -x^3 + x^2 y + x^2 + \frac{1}{5} xy + \frac{1}{5} x - \frac{1}{5} y - \frac{1}{5} \\ x^3 - x^2 y + x^2 + \frac{1}{5} xy - \frac{1}{5} x + \frac{1}{5} y - \frac{1}{5} \end{pmatrix}.$$

Next, we use the *periodic* basis functions constructed in (3.9) to solve the *periodic* finite element approximation problem (3.14) (see FIGURE 3), and have

$$z^* = \begin{pmatrix} \frac{5}{14} x^2 y - \frac{5}{14} xy^2 + \frac{3}{14} x^2 - \frac{4}{7} xy + \frac{3}{14} y^2 - \frac{3}{14} x + \frac{3}{14} y + \frac{1}{7} \\ -\frac{5}{14} x^2 y + \frac{5}{14} xy^2 + \frac{3}{14} x^2 - \frac{4}{7} xy + \frac{3}{14} y^2 + \frac{3}{14} x - \frac{3}{14} y + \frac{1}{7} \end{pmatrix}.$$

Here, $\psi^* = x^3y - I_h(x^3y) - z^*$ is not in $\Phi_4(\hat{K})$ yet, since its integral over $\hat{K}$ is not 0. Note that a constant function is periodic. We can let $z = z^* + c$ and solve (3.15) for c. It turns out that $c = -\frac{2}{21}$. Put $z = z^* - \frac{2}{21}$. Then, we obtain $\psi = x^3y - I_h(x^3y) - z \in \Phi_4(\hat{K})$ corresponding to x^3y, which is

$$\psi = \begin{pmatrix} x^3y + x^3 - \frac{19}{14}x^2y + \frac{5}{14}xy^2 - \frac{17}{14}x^2 + \frac{13}{35}xy - \frac{3}{14}y^2 + \frac{1}{70}x - \frac{1}{70}y + \frac{16}{105} \\ x^3y - x^3 + \frac{19}{14}x^2y - \frac{5}{14}xy^2 - \frac{17}{14}x^2 + \frac{13}{35}xy - \frac{3}{14}y^2 - \frac{1}{70}x + \frac{1}{70}y + \frac{16}{105} \end{pmatrix}.$$

This systematic process is more suitable for computer implementation than the orthogonal decomposition process. Once the code is set, we can feed the program with different $(n+1)^{th}$ order polynomials to get the corresponding functions in $\Phi_{n+1}(\hat{K})$. In particular, this process offers us an approach for ψ_{n+1}^{Re} and ψ_{n+1}^{Im}. Letting u be the harmonic polynomial $Re(z^{n+1})$ or $Im(z^{n+1})$, the process will yield ψ_{n+1}^{Re} or ψ_{n+1}^{Im}, respectively. □

3.1.3. **Superconvergent Points**

After specification of basis functions of $\Phi_{n+1}(\hat{K})$, we are ready to locate superconvergent points for the Poisson equation.

Theorem 3.4. *Consider superconvergence for the Poisson equation on l_{12}.*
(i) For odd n, the midpoint of l_{12} is x-derivative superconvergent point;
(ii) If $n = 2$, the two Gaussian points on l_{12} are x-derivative superconvergent points;
(iii) For even n, the endpoints and midpoint of l_{12} are function value superconvergent points.

Similar results hold on the other sides. In particular, we refer to tangential derivative superconvergence on each side, including the diagonal side.

Proof. Clearly, $\varsigma_k^{12}|_{l_{12}} = \phi_k(x)$, which will cancel $\phi_k(x)y|_{l_{12}}$ since $y = -1$ on l_{12}. The other side modes and all internal modes are identically 0 on l_{12}. Note that $\phi_j(y) = 0$ on l_{12}. Therefore, restricted on l_{12}, the basis functions of $\Phi_{n+1}(\hat{K})$ are classified in two types: $\phi_{n+1}(x) + r_n^0$ and r_n^j for $j = 1, \ldots, n+1$.

(i) Suppose $n = 2m+1$. From Theorem 3.3,

$$r_{2m+1}^j|_{l_{12}} = c_0^j + \sum_{i=1}^{m} c_i^j \varsigma_{2i}^{12}|_{l_{12}} = c_0^j + \sum_{i=1}^{m} c_i^j \phi_{2i}(x), \ ^1$$

where c_i^js are constants, $j = 0, \ldots, 2m+2$. Also, $\phi_{n+1}(x) = \phi_{2(m+1)}(x)$. Thus, the basis functions of $\Phi_{n+1}(\hat{K})$ restricted on l_{12} are all linear combinations of even order $\phi_k(x)$s, whose derivatives are odd order Legendre polynomials, which have a common zero at the midpoint of l_{12}.

(ii) The superconvergence is verified directly.

(iii) Suppose $n = 2m$. From Theorem 3.3,

$$r_{2m}^j|_{l_{12}} = \sum_{i=2}^{m} c_i^j \varsigma_{2i-1}^{12}|_{l_{12}} = \sum_{i=2}^{m} c_i^j \phi_{2i-1}(x),$$

where c_i^js are constants, $j = 0, \ldots, 2m+1$. Also, $\phi_{n+1}(x) = \phi_{2m+1}(x)$. Therefore, the basis functions of $\Phi_{n+1}(\hat{K})$ are all linear combinations of odd order $\phi_k(x)$s, which have common zeros at two endpoints and midpoint of l_{12}. □

[1] If $m = 0$, then r_1^js are constants.

Theorem 3.4 predicts superconvergence at some specific points on the element edges. Whether these are all superconvergent points should be justified by Theorems 3.1 and 3.2. Namely, we need to determine the intersections of the contours induced from the basis functions of $\Phi_{n+1}(\hat{K})$, which are solutions of a system of polynomial equations. When n is small (eg. $n = 1$ or 2), the system can be solved analytically. When n is large, this can be done accurately with help of computation softwares (MATLAB, MAPLE) and numerical methods (eg. Newton's method), which are available in many reference books (eg. [8]). We have the following results for n up to 8.

Proposition 3.1. *For the regular mesh, superconvergent points of function values for the Poisson equation in $\hat{T}_1$ are:*
(i) If n is odd, there is no superconvergent point;
(ii) If n is even, the vertices and midpoints of edges are the only superconvergent points.

Proposition 3.2. *For the regular mesh, superconvergent points of $\frac{\partial u}{\partial x}$ (or $\frac{\partial u}{\partial y}$) for the Poisson equation in $\hat{T}_1$ are:*
(i) If n is odd, the midpoint of l_{12} (or l_{23}) is the only superconvergent point;
(ii) If $n = 2$, the two Gaussian points on l_{12} (or l_{23}) are the only superconvergent points;
(iii) If n is even and greater than 2, there is no superconvergent point.

Remark 3.4. Theorem 3.4 coincides with the results from the symmetry principles [14, 17], which are sufficient. Propositions 3.1 and 3.2 are conclusive; i.e. they indicate that there are no other superconvergent points. Proposition 3.2 also agrees with the corresponding results in [2]. Note that the case $n = 2$ was reported much earlier [1, 20]. □

Now, we consider the Laplace equation. We first determine ψ_{n+1}^{Re} and ψ_{n+1}^{Im}. These functions can be obtained from basis functions of $\Phi_{n+1}(\hat{K})$ by adding the periodic polynomials corresponding to terms in $Re(z^{n+1})$ and $Im(z^{n+1})$, respectively; they can also be derived from the process described in Remark 3.1. For $n = 1, \ldots, 4$, we have

$$\psi_2^{Re} = x^2 - y^2,$$
$$\psi_2^{Im} = \begin{pmatrix} xy + x - y - \frac{2}{3} \\ xy - x + y - \frac{2}{3} \end{pmatrix};$$

$$\psi_3^{Re} = \begin{pmatrix} x^3 - 3xy^2 - 3xy + 3y^2 - x + 3y \\ x^3 - 3xy^2 + 3xy - 3y^2 - x + 3y \end{pmatrix},$$
$$\psi_3^{Im} = \begin{pmatrix} y^3 - 3yx^2 + 3yx - 3x^2 - y + 3x \\ y^3 - 3yx^2 - 3yx + 3x^2 - y + 3x \end{pmatrix};$$

$$\psi_4^{Re} = \begin{pmatrix} x^4 - 6x^2y^2 + y^4 - 6x^2y + 6xy^2 - 2x^2 + 8xy - 2y^2 + 2x - 2y - \frac{8}{15} \\ x^4 - 6x^2y^2 + y^4 + 6x^2y - 6xy^2 - 2x^2 + 8xy - 2y^2 - 2x + 2y - \frac{8}{15} \end{pmatrix},$$
$$\psi_4^{Im} = \begin{pmatrix} x^3y - xy^3 + x^3 - x^2y - xy^2 + y^3 - x^2 + y^2 \\ x^3y - xy^3 - x^3 + x^2y + xy^2 - y^3 - x^2 + y^2 \end{pmatrix};$$

$$\psi_5^{Re} = \begin{pmatrix} x^5 - 10x^3y^2 + 5xy^4 - \frac{155}{12}x^3y + \frac{25}{2}x^2y^2 + \frac{65}{12}xy^3 - 5y^4 - \frac{135}{28}x^3 + \frac{75}{4}x^2y \\ -\frac{85}{28}xy^2 - \frac{65}{12}y^3 + \frac{25}{4}x^2 - \frac{95}{14}xy + \frac{15}{28}y^2 - \frac{17}{7}x + \frac{20}{21}y \\ x^5 - 10x^3y^2 + 5xy^4 + \frac{155}{12}x^3y - \frac{25}{2}x^2y^2 - \frac{65}{12}xy^3 + 5y^4 - \frac{135}{28}x^3 + \frac{75}{4}x^2y \\ -\frac{85}{28}xy^2 - \frac{65}{12}y^3 - \frac{25}{4}x^2 + \frac{95}{14}xy - \frac{15}{28}y^2 - \frac{17}{7}x + \frac{20}{21}y \end{pmatrix},$$

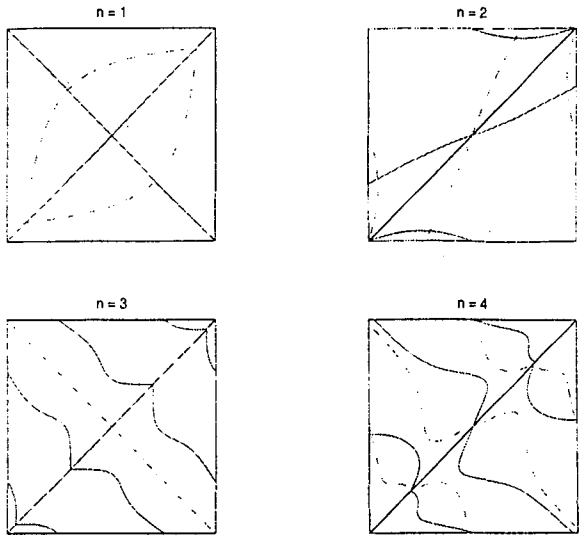

Figure 4: Contours $\psi_{n+1}^{Re} = 0$ (solid) and $\psi_{n+1}^{Im} = 0$ (dashed), $n = 1, \ldots, 4$.

$$\psi_5^{Im} = \begin{pmatrix} y^5 - 10y^3x^2 + 5yx^4 + \frac{155}{12}y^3x - \frac{25}{2}y^2x^2 - \frac{65}{12}yx^3 + 5x^4 - \frac{135}{28}y^3 + \frac{75}{4}y^2x \\ -\frac{85}{28}yx^2 - \frac{65}{12}x^3 - \frac{25}{4}y^2 + \frac{95}{14}yx - \frac{15}{28}x^2 - \frac{17}{7}y + \frac{20}{21}x \\ y^5 - 10y^3x^2 + 5yx^4 - \frac{155}{12}y^3x + \frac{25}{2}y^2x^2 + \frac{65}{12}yx^3 - 5x^4 - \frac{135}{28}y^3 + \frac{75}{4}y^2x \\ -\frac{85}{28}yx^2 - \frac{65}{12}x^3 + \frac{25}{4}y^2 - \frac{95}{14}yx + \frac{15}{28}x^2 - \frac{17}{7}y + \frac{20}{21}x \end{pmatrix}.$$

ψ_{n+1}^{Re} and ψ_{n+1}^{Im} for $n = 5, \ldots, 8$ are provided in [13].

By Theorem 3.2 (i), the function value superconvergent points are the intersections of the contours $\psi_{n+1}^{Re} = 0$ and $\psi_{n+1}^{Im} = 0$. For instance, when $n = 1$, the superconvergent points in $\hat{T}_1$ can be obtained by solving

$$\begin{cases} x^2 - y^2 = 0, \\ xy + x - y - \frac{2}{3} = 0, \end{cases}$$

in $\hat{T}_1$. From the first equation, we have $x = y$ or $x = -y$. Substituting these into the second equation, we obtain $(\pm\frac{\sqrt{6}}{3}, \pm\frac{\sqrt{6}}{3})$ and $(1 - \frac{\sqrt{3}}{3}, -1 + \frac{\sqrt{3}}{3})$ in $\hat{T}_1$, which are desired superconvergent points.

When $n = 2$, we need to solve

$$\begin{cases} x^3 - 3xy^2 - 3xy + 3y^2 - x + 3y = 0, \\ y^3 - 3yx^2 + 3yx - 3x^2 - y + 3x = 0, \end{cases}$$

or equivalently, to solve

$$\begin{cases} (x-1)(x^2 - 3y^2 + x - 3y) = 0, \\ (y+1)(y^2 - 3x^2 - y + 3x) = 0. \end{cases}$$

It is straightforward to verify that the solutions (superconvergent points) in $\hat{T}_1$ are the vertices, the midpoints of edges, and $(\frac{1}{4} \pm \frac{\sqrt{7}}{4}, -\frac{1}{4} \pm \frac{\sqrt{7}}{4})$.

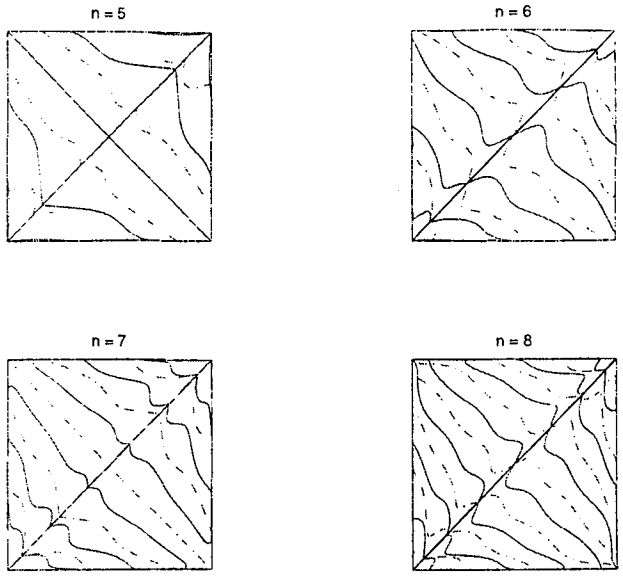

Figure 5: Contours $\psi_{n+1}^{Re} = 0$ (solid) and $\psi_{n+1}^{Im} = 0$ (dashed), $n = 5, \ldots, 8$.

For each n, we need to solve a pair of polynomial equations. When n is large, numerical methods are required. Although how to efficiently solve a polynomial equation system is an interesting problem, it is not our focus. Here, we simply use the Newton method. With

TABLE 1(a). Function Value Superconvergent Points for the Regular Pattern (in $\hat{T}_1$, $n = 1, \ldots, 4$)

	$n=1$	$n=2$	$n=3$	$n=4$
1	−0.8164965809277260	−1.0000000000000000	−0.5193296223592281	−1.0000000000000000
	−0.8164965809277260	−1.0000000000000000	−1.0000000000000000	−1.0000000000000000
2	0.4226497308103742	0.0000000000000000	0.5193296223592281	−0.9511897312113419
	−0.4226497308103742	−1.0000000000000000	−1.0000000000000000	−1.0000000000000000
3	0.8164965809277260	1.0000000000000000	−0.9173685331054181	0.0000000000000000
	0.8164965809277260	−1.0000000000000000	−0.9173685331054181	−1.0000000000000000
4		−0.4114378277661476	1.0000000000000000	0.9511897312113419
		−0.9114378277661476	−0.5193296223592281	−1.0000000000000000
5		0.0000000000000000	−0.3980389107461900	1.0000000000000000
		0.0000000000000000	−0.3980389107461900	−1.0000000000000000
6		1.0000000000000000	0.3980389107461900	−0.0703819804091844
		0.0000000000000000	0.3980389107461900	−0.9828670086417396
7		0.9114378277661476	1.0000000000000000	1.0000000000000000
		0.4114378277661476	0.5193296223592281	−0.9511897312113419
8		1.0000000000000000	0.9173685331054181	−0.6074928962939559
		1.0000000000000000	0.9173685331054181	−0.6074928962939559
9				0.0000000000000000
				0.0000000000000000
10				1.0000000000000000
				0.0000000000000000
11				0.9828670086417396
				0.0703819804091844
12				0.6074928962939559
				0.6074928962939559
13				1.0000000000000000
				0.9511897312113419
14				1.0000000000000000
				1.0000000000000000

TABLE 1(b). Function Value Superconvergent Points for the Regular Pattern (in $\hat{T}_1$, $n = 5, \ldots, 8$)

	$n = 5$	$n = 6$	$n = 7$	$n = 8$
1	−1.0000000000000000	−1.0000000000000000	−0.7283987607253135	−1.0000000000000000
	−1.0000000000000000	−1.0000000000000000	−1.0000000000000000	−1.0000000000000000
2	−0.3779644730092272	−0.5860928017843374	−0.2616196034057031	−0.9985182765124761
	−1.0000000000000000	−1.0000000000000000	−1.0000000000000000	−1.0000000000000000
3	0.3779644730092272	0.0000000000000000	0.2616196034057031	−0.8415029196420455
	−1.0000000000000000	−1.0000000000000000	−1.0000000000000000	−1.0000000000000000
4	1.0000000000000000	0.5860928017843374	0.7283987607253135	−0.4499077973241774
	−1.0000000000000000	−1.0000000000000000	−1.0000000000000000	−1.0000000000000000
5	−0.5138908967122077	1.0000000000000000	−0.9981396004694932	0.0000000000000000
	−0.9855536016972144	−1.0000000000000000	−0.9981396004694932	−1.0000000000000000
6	−0.7520955703220618	−0.8001753718755459	−0.8677139861534285	0.4499077973241774
	−0.7520955703220618	−0.9926259609529336	−0.8677139861534285	−1.0000000000000000
7	1.0000000000000000	−0.8258100260262924	−0.7946854333174225	0.8415029196420455
	−0.3779644730092272	−0.8258100260262924	−0.8546890237923378	−1.0000000000000000
8	−0.2738197456392299	1.0000000000000000	1.0000000000000000	0.9985182765124761
	−0.2738197456392299	−0.5860928017843374	−0.7283987607253135	−1.0000000000000000
9	0.2738197456392299	−0.4616469028358420	−0.5861275452213199	1.0000000000000000
	0.2738197456392299	−0.4616469028358420	−0.5861275452213199	−1.0000000000000000
10	1.0000000000000000	1.0000000000000000	1.0000000000000000	1.0000000000000000
	0.3779644730092272	0.0000000000000000	−0.2616196034057031	−0.9985182765124761
11	0.9855536016972144	0.0000000000000000	−0.2065452580134060	−0.5111908039811860
	0.5138908967122077	0.0000000000000000	−0.2065452580134060	−0.9975720711785237
12	0.7520955703220618	0.4616469028358420	0.2065452580134060	0.9834451655126653
	0.7520955703220618	0.4616469028358420	0.2065452580134060	−0.9834451655126653
13	1.0000000000000000	1.0000000000000000	1.0000000000000000	0.8208569446704606
	1.0000000000000000	0.5860928017843374	0.2616196034057031	−0.9479254719651945
14		0.9926259609529336	0.5861275452213199	−0.8949872464334571
		0.8001753718755459	0.5861275452213199	−0.8949872464334571
15		0.8258100260262924	1.0000000000000000	−0.8006759120160012
		0.8258100260262924	0.7283987607253135	−0.8857531090977044
16		1.0000000000000000	0.8546890237923378	1.0000000000000000
		1.0000000000000000	0.7946854333174225	−0.8415029196420455
17			0.8677139861534285	0.9479254719651945
			0.8677139861534285	−0.8208569446704606
18			0.9981396004694932	−0.6718072968265310
			0.9981396004694932	−0.6718072968265310
19				1.0000000000000000
				−0.4499077973241774
20				−0.3593519628863694
				−0.3593519628863694
21				0.0000000000000000
				0.0000000000000000
22				1.0000000000000000
				0.0000000000000000
23				1.0000000000000000
				0.4499077973241774
24				0.9975720711785237
				0.5111908039811860
25				0.6718072968265310
				0.6718072968265310
26				0.3593519628863694
				0.3593519628863694
27				0.8857531090977044
				0.8006759120160012
28				1.0000000000000000
				0.8415029196420455
29				0.8949872464334571
				0.8949872464334571
30				1.0000000000000000
				0.9985182765124761
31				1.0000000000000000
				1.0000000000000000

help of MAPLE and MATLAB, we obtain function value superconvergent points for $n = 1, \ldots, 8$, which are listed in TABLE 1 with 16 digits of accuracy. In FIGURE 4 and FIGURE 5, we plot the contours for cases $n = 1, \ldots, 8$ by MATLAB.

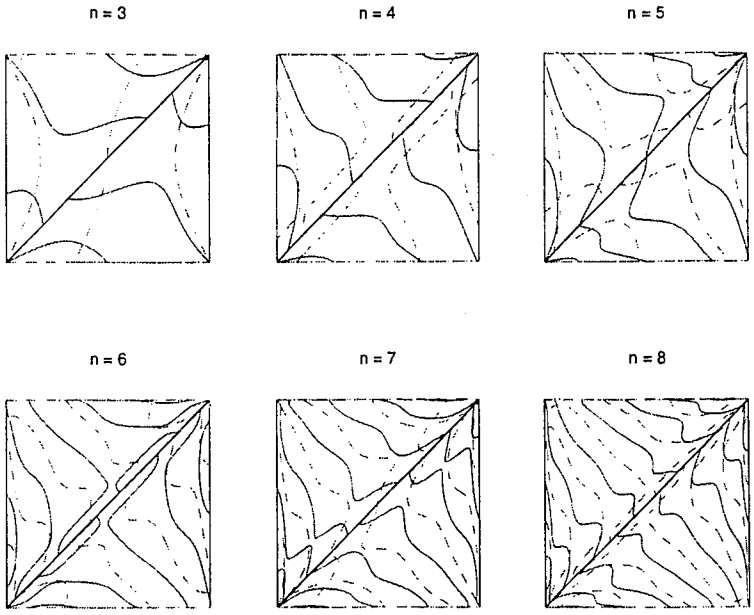

Figure 6: Contours $\frac{\partial \psi_{n+1}^{Re}}{\partial x} = 0$ (solid) and $\frac{\partial \psi_{n+1}^{Im}}{\partial x} = 0$ (dashed), $n = 3, \ldots, 8$.

By Theorem 3.2 (ii), the x-derivative superconvergent points are the intersections of the contours $\frac{\partial \psi_{n+1}^{Re}}{\partial x} = 0$ and $\frac{\partial \psi_{n+1}^{Im}}{\partial x} = 0$. As an example, we consider the case for $n = 2$. The x-derivative superconvergent points in $\hat{T}_1$ are the solutions of the system

$$\begin{cases} \frac{\partial \psi_3^{Re}|_{\hat{T}_1}}{\partial x} = 3x^2 - 3y^2 - 3y - 1 = 0, \\ \frac{\partial \psi_3^{Im}|_{\hat{T}_1}}{\partial x} = -3(y+1)(2x-1) = 0. \end{cases}$$

Solve this system, we obtain four superconvergent points: $(\pm\frac{\sqrt{3}}{3}, -1)$ and $(\frac{1}{2}, -\frac{1}{2} \pm \frac{\sqrt{6}}{6})$.

TABLE 2(a). Derivative Superconvergent Points for the Regular Pattern (in $\hat{T}_1$, $n = 1, \ldots, 4$)

	$n=1$	$n=2$	$n=3$	$n=4$
1	0.0000000000000000 −1.0000000000000000	−0.5773502691896258 −1.0000000000000000	−1.0000000000000000 −1.0000000000000000	−0.9762047562738165 −1.0000000000000000
2		0.5773502691896258 −1.0000000000000000	0.0000000000000000 −1.0000000000000000	−0.4357538487328842 −1.0000000000000000
3		0.5000000000000000 −0.9082482904638630	1.0000000000000000 −1.0000000000000000	0.4357538487328842 −1.0000000000000000
4		0.5000000000000000 −0.0917517095361370	−0.2495636041803519 −0.8282349823299942	0.9762047562738165 −1.0000000000000000
5			−0.0569628865629212 −0.3516533583837684	0.4106905181904221 −0.9856261245779083
6			0.7276352521634410 0.3648132073349060	−0.7609910954777545 −0.9550014625469050
7				−0.3809408103995712 −0.5597762653529965
8				0.2804554307532021 0.0392284719195946
9				0.8126724617779161 0.5742483905274366

TABLE 2(b). Derivative Superconvergent Points for the Regular Pattern (in $\hat{T}_1$, $n = 5, \ldots, 8$)

	$n=5$	$n=6$	$n=7$	$n=8$
1	−1.0000000000000000 −1.0000000000000000	−0.7802941074859182 −1.0000000000000000	−1.0000000000000000 −1.0000000000000000	−0.9992622651115187 −1.0000000000000000
2	−0.6546536707079771 −1.0000000000000000	−0.2902920033562139 −1.0000000000000000	−0.8724199011562877 −1.0000000000000000	−0.9054011724682842 −1.0000000000000000
3	0.0000000000000000 −1.0000000000000000	0.2902920033562139 −1.0000000000000000	−0.4887571135712024 −1.0000000000000000	−0.6276397150039605 −1.0000000000000000
4	0.6546536707079771 −1.0000000000000000	0.7802941074859182 −1.0000000000000000	0.0000000000000000 −1.0000000000000000	−0.2219131070745645 −1.0000000000000000
5	1.0000000000000000 −1.0000000000000000	−0.4296804190843017 −0.9794457423195006	0.4887571135712024 −1.0000000000000000	0.2219131070745645 −1.0000000000000000
6	−0.0718949366554462 −0.9793960316434498	0.9743835257461033 −0.8404683252781456	0.8724199011562877 −1.0000000000000000	0.6276397150039605 −1.0000000000000000
7	−0.5342467051008834 −0.6850142752143384	−0.4385937672691014 −0.7471180163419970	1.0000000000000000 −1.0000000000000000	0.9054011724682842 −1.0000000000000000
8	−0.0530467624549399 −0.2251798300015251	−0.2682485061163367 −0.4043522076362224	−0.6759991164966385 −0.9887878384682518	0.9992622651115187 −1.0000000000000000
9	0.4712605850961711 0.2851933532419337	0.1747948038384324 0.0312903099656319	0.9675399749272883 −0.9442318436480794	−0.2284265164539444 −0.9993186201946292
10	0.8687318398155543 0.4160368104008867	0.5930068961438869 0.4069367800853346	−0.5526058285230658 −0.8204988182282370	−0.8604358636216127 −0.9979626530937577
11		0.9113920897175050 0.5542101472898292	−0.4101259591003691 −0.5269703699170518	0.8819561225984842 −0.9429515274310050
12			−0.0458573784465860 −0.1593499763070021	0.9779759193542496 −0.8982852264369150
13			0.3378030147268201 0.2035258346590941	−0.6244716257411005 −0.8619397552651930
14			0.6826097321374772 0.4053072896642744	0.9731368926379180 −0.7072548415558784
15			0.9343855681592637 0.6390587782077723	−0.4628273322658001 −0.5991284868687132
16				−0.2109347493642553 −0.3065003891547965
17				0.1284564982199144 0.0272532561080603
18				0.4429632529165919 0.2637028329059902
19				0.7540612856604619 0.4936457864836795
20				0.9467527974578255 0.6378027221999435

When $n = 3$, The superconvergent points are the solutions of the system

$$\begin{cases} \frac{\partial \psi_4^{Re}|_{\hat{T}_1}}{\partial x} = 4x^3 - 12xy^2 - 12xy + 6y^2 - 4x + 8y + 2 = 0, \\ \frac{\partial \psi_4^{Im}|_{\hat{T}_1}}{\partial x} = (y+1)(3x^2 - y^2 - 2x) = 0. \end{cases}$$

From the second equation, we have $y + 1 = 0$ or $3x^2 - y^2 - 2x = 0$. If we substitute $y = -1$ into the first equation, the system can be easily solved. However, when substituting $y = \pm\sqrt{3x^2 - 2x}$ into the first equation, we have

$$(x-1)(256x^5 - 416x^4 + 173x^3 + 21x^2 - 17x - 1) = 0,$$

provided $3x^2 - 2x \geq 0$. To solve a polynomial equation of degree 5, numerical methods are required.

Following a similar process for function value superconvergent points, the x-derivative superconvergent points can be located in $\hat{K}$. In TABLE 2, the superconvergent points in $\hat{T}_1$

are summarized for $n = 1, \ldots, 8$ with 16 digits of accuracy. Since the cases for $n = 1, 2$ are trivial, we plot only the contours for cases $n = 3, \ldots, 8$ by MATLAB in FIGURE 6.

Remark 3.5. In order to compare our results with data in $[2]$[2], where the master cell is $\kappa = [0,1]^2$, we map $\hat{K}$ to κ by affine mapping $x^\kappa = (x^{\hat{K}} + 1)/2$ and $y^\kappa = (y^{\hat{K}} + 1)/2$. Note that the nodal shape functions defined in $\hat{K}$ are mapped to those defined in κ under the same affine mapping. We then conclude that $\Phi_{n+1}(\hat{K})$ is transferred to $\Phi_{n+1}(\kappa)$ because of its construction. Since affine mappings preserve zeros for derivatives, the derivative superconvergence points in $\hat{K}$ are mapped to those in κ. We found that the first 9 digits of the superconvergent points listed in [2] are the same as those obtained here[3]. □

By Theorem 3.2 (ii), we can also determine the y-derivative superconvergent points. It can be shown that $\frac{\partial \psi_{2k}^{Re}(-y,-x)}{\partial y} = (-1)^{k+1} \frac{\partial \psi_{2k}^{Re}(x,y)}{\partial x}$, $\frac{\partial \psi_{2k}^{Im}(-y,-x)}{\partial y} = (-1)^k \frac{\partial \psi_{2k}^{Im}(x,y)}{\partial x}$; and $\frac{\partial \psi_{2k+1}^{Re}(-y,-x)}{\partial y} = \frac{\partial \psi_{2k+1}^{Im}(x,y)}{\partial x}$, $\frac{\partial \psi_{2k+1}^{Im}(-y,-x)}{\partial y} = \frac{\partial \psi_{2k+1}^{Re}(x,y)}{\partial x}$ for $k = 1, 2, \ldots$ Therefore, the y-derivative superconvergent points for the Laplace equation turn out to be the symmetry points of the x-derivative superconvergent points about $y = -x$.

3.2. CHEVRON PATTERN

We observe that a period occupies only half of the square in the Chevron pattern. Therefore, we set $\hat{K} = [-1,1] \times [0,1]$ here. Partition $\hat{K}$ into four triangular elements (see FIGURE 7).

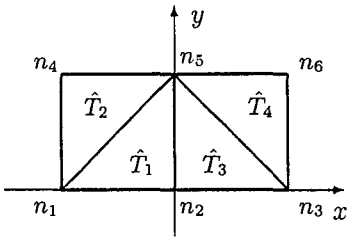

Figure 7: Partition of $\hat{K}$ for the Chevron Pattern

We still use $P_n^w(\hat{K})$ and $PP_n^w(\hat{K})$ to denote the counterpart spaces defined in Section 3.1. The definitions of the spaces are adjusted accordingly due to the changing of the reference cell.

The hierarchic basis functions are used for $V_n(\hat{K})$. Let ν_i be the linear nodal shape function corresponding to vertex n_i, which are defined in (3.20). The side modes and internal modes are defined as in (3.6) and (3.7), respectively.

The periodic basis functions are constructed from ν_i, ς_k^{ij} and $\iota_{k,j}^i$ similar to those in Section 3.1. Notice that $\nu_1 + \nu_3 + \nu_4 + \nu_6$ and $\nu_2 + \nu_5$ are two periodic basis functions in this case.

[2]In [2], TABLE I, superconvergent points are given for n up to 7.

[3]Some of the 10^{th} decimal places in [2] are not accurate in the "round-off" sense.

$$\nu_1 = \begin{cases} -x & \text{in } \hat{T}_1, \\ 1-y & \text{in } \hat{T}_2, \\ 0 & \text{in } \hat{T}_3,\ \hat{T}_4; \end{cases} \qquad \nu_4 = \begin{cases} -x+y-1 & \text{in } \hat{T}_2, \\ 0 & \text{in } \hat{T}_1,\ \hat{T}_3,\ \hat{T}_4; \end{cases}$$

$$\nu_2 = \begin{cases} 1+x-y & \text{in } \hat{T}_1, \\ 1-x-y & \text{in } \hat{T}_3, \\ 0 & \text{in } \hat{T}_2,\ \hat{T}_4; \end{cases} \qquad \nu_5 = \begin{cases} y & \text{in } \hat{T}_1, \\ x+1 & \text{in } \hat{T}_2, \\ y & \text{in } \hat{T}_3, \\ -x+1 & \text{in } \hat{T}_4; \end{cases} \tag{3.20}$$

$$\nu_3 = \begin{cases} x & \text{in } \hat{T}_3, \\ 1-y & \text{in } \hat{T}_4, \\ 0 & \text{in } \hat{T}_1,\ \hat{T}_2; \end{cases} \qquad \nu_6 = \begin{cases} x+y-1 & \text{in } \hat{T}_4, \\ 0 & \text{in } \hat{T}_1,\ \hat{T}_2,\ \hat{T}_3. \end{cases}$$

It is straightforward to verify that

$$\dim P_n^w(\hat{K}) = (2n+1)(n+1), \quad \dim PP_n^w(\hat{K}) = 2n^2. \tag{3.21}$$

Theorems 3.1 and 3.2 still hold for the Chevron mesh. To determine the space $\Phi_{n+1}(\hat{K})$, we can either make an orthogonal decomposition of $PP_{n+1}^w(\hat{K})$, or solve a periodic finite element approximation problem, as described in Remark 3.1.

If the first approach is adopted, we need to define $\Psi_n(\hat{K})$ as in (3.11). The difference here is that the integral domain consists of 4 elements instead of 2. By the Gram-Schmidt process, we obtain a list of $\Psi_n(\hat{K})$, where $PP_n^w(\hat{K})$ can be decomposed as in (3.12). Based on $\Psi_n(\hat{K})$, we are able to construct $\Phi_n(\hat{K})$.

Remark 3.6. From the geometrical point of view, the left side of the y-axis is one patch of the regular mesh. In fact, under the corresponding affine mapping ($x^{Rg} = 2x^{Ch} + 1$ and $y^{Rg} = 2y^{Ch} - 1$), the shape functions on $\hat{T}_1$ and $\hat{T}_2$ defined in (3.20) are mapped to the ones of the regular pattern. Similar situation happens to the right side of the y-axis. We thus conclude that similar symmetry results as in Lemma 3.3 hold for the Chevron pattern. Hence, we need to work only on superconvergent points in the first element. Superconvergent points in the other elements can be obtained by symmetry. □

In the following, basis functions of $\Phi_{n+1}(\hat{K})$ in $\hat{T}_1$ are provided for $n = 1, \ldots, 4$. For cases of $n = 5, \ldots, 8$, the reader is referred to [13]. To simplify notations, let B_{n+1}^j be the j^{th} basis function of $\Phi_{n+1}(\hat{K})$. Denote θ_n the column vector consists of all nodal shape functions, side modes and internal modes of order $\leq n$ in $\hat{T}_1$. The length of θ_n is $(n+1)(n+2)/2$. In particular, we assign ν_1, ν_2 and ν_5 the first 3 entries of θ_n; assign the side modes ς_k^{12}, ς_k^{25} and ς_k^{51} as the $(k(k+1)/2+1)^{th}$ to the $(k(k+1)/2+3)^{th}$ entries, $k = 2, \ldots, n$; and assign the internal modes $\iota_{k,1}^1$ to $\iota_{k,k-2}^1$ as the $(k(k+1)/2+4)^{th}$ to the $((k+1)(k+2)/2)^{th}$ entries, $k = 3, \ldots, n$. For instance,

$$\begin{aligned} \theta_1 &= [\nu_1, \nu_2, \nu_5]^T, \\ \theta_2 &= [\theta_1,\ \varsigma_2^{12}, \varsigma_2^{25}, \varsigma_2^{51}]^T, \\ \theta_3 &= [\theta_2,\ \varsigma_3^{12}, \varsigma_3^{25}, \varsigma_3^{51}, \iota_{3,1}^1]^T, \\ \theta_4 &= [\theta_3,\ \varsigma_4^{12}, \varsigma_4^{25}, \varsigma_4^{51}, \iota_{4,1}^1, \iota_{4,2}^1]^T. \end{aligned} \tag{3.22}$$

Then, in element $\hat{T}_1$, the basis functions of $\Phi_{n+1}(\hat{K})$ can be expressed as

$$
\begin{aligned}
B_2^1 &= \phi_2(x) + [\tfrac{1}{12}, \tfrac{7}{12}, \tfrac{7}{12}]\ \theta_1,\\
B_2^2 &= xy,\\
B_2^3 &= \phi_2(y) + [\tfrac{7}{12}, \tfrac{7}{12}, \tfrac{1}{12}]\ \theta_1;
\end{aligned}
$$

$$
\begin{aligned}
B_3^1 &= \phi_3(x) + [0, 0, 0, \tfrac{3}{8}, 0, \tfrac{3}{8}]\ \theta_2,\\
B_3^2 &= \phi_2(x)y + [-\tfrac{1}{160}, \tfrac{1}{160}, \tfrac{81}{160}, 0, \tfrac{3}{160}, \tfrac{1}{8}]\ \theta_2,\\
B_3^3 &= x\phi_2(y) + [-\tfrac{1}{2}, 0, 0, 0, 0, -\tfrac{1}{8}]\ \theta_2,\\
B_3^4 &= \phi_3(y) + [-\tfrac{3}{160}, \tfrac{3}{160}, \tfrac{3}{160}, 0, -\tfrac{51}{160}, -\tfrac{3}{8}]\ \theta_2;
\end{aligned}
$$

$$
\begin{aligned}
B_4^1 &= \phi_4(x) + [\tfrac{1}{224}, -\tfrac{27}{224}, -\tfrac{27}{224}, -\tfrac{39}{224}, \tfrac{3}{224}, -\tfrac{1791}{10304}, \tfrac{5}{16}, \tfrac{15}{5152}, \tfrac{5}{16}, -\tfrac{5735}{5152}]\ \theta_3,\\
B_4^2 &= \phi_3(x)y + [0, 0, 0, \tfrac{1}{336}, 0, \tfrac{593}{3360}, 0, 0, \tfrac{1}{8}, -\tfrac{23}{112}]\ \theta_3,\\
B_4^3 &= \phi_2(x)\phi_2(y) + [\tfrac{1}{504}, -\tfrac{125}{504}, \tfrac{1}{504}, \tfrac{11}{84}, \tfrac{11}{84}, \tfrac{2173}{7728}, 0, \tfrac{3}{1288}, 0, \tfrac{187}{1288}]\ \theta_3,\\
B_4^4 &= x\phi_3(y) + [0, 0, 0, \tfrac{1}{336}, 0, \tfrac{593}{3360}, 0, 0, -\tfrac{1}{8}, -\tfrac{23}{112}]\ \theta_3,\\
B_4^5 &= \phi_4(y) + [-\tfrac{27}{224}, -\tfrac{27}{224}, \tfrac{1}{224}, \tfrac{3}{224}, -\tfrac{39}{224}, -\tfrac{1761}{10304}, 0, -\tfrac{1445}{5152}, -\tfrac{5}{16}, -\tfrac{5585}{5152}]\ \theta_3;
\end{aligned}
$$

$$
\begin{aligned}
B_5^1 &= \phi_5(x) + [0, 0, 0, -\tfrac{1}{16}, 0, -\tfrac{1}{16}, -\tfrac{235}{768}, 0, -\tfrac{2135}{6912}, -\tfrac{185}{576}, \tfrac{7}{32}, 0, \tfrac{7}{32}, -\tfrac{24955}{6912}, \tfrac{35}{6912}]\ \theta_4,\\
B_5^2 &= \phi_4(x)y + [-\tfrac{25}{26208}, \tfrac{25}{26208}, -\tfrac{3251}{26208}, 0, \tfrac{25}{8736}, -\tfrac{1}{8}, \tfrac{245}{44928}, \tfrac{25}{16128}, \tfrac{8263}{139776}, -\tfrac{867}{2912}, 0, \tfrac{85}{44928}, \tfrac{3}{32}, -\tfrac{8405}{14976}, -\tfrac{18335}{89856}]\ \theta_4,\\
B_5^3 &= \phi_3(x)\phi_2(y) + [0, 0, 0, -\tfrac{3}{16}, 0, -\tfrac{11}{80}, \tfrac{257}{4032}, 0, \tfrac{181}{1344}, -\tfrac{277}{2016}, 0, 0, \tfrac{1}{80}, \tfrac{77}{576}, -\tfrac{13}{576}]\ \theta_4,\\
B_5^4 &= \phi_2(x)\phi_3(y) + [-\tfrac{25}{104832}, \tfrac{25}{104832}, \tfrac{25}{104832}, 0, \tfrac{6577}{34944}, \tfrac{11}{80}, \tfrac{29}{22464}, \tfrac{257}{4032}, \tfrac{7115}{52416}, \tfrac{2515}{17472}, 0, \tfrac{11}{11232}, -\tfrac{1}{80}, -\tfrac{83}{14976}, \tfrac{6007}{44928}]\ \theta_4,\\
B_5^5 &= x\phi_4(y) + [\tfrac{1}{8}, 0, 0, 0, 0, \tfrac{1}{8}, \tfrac{25}{16128}, 0, \tfrac{2657}{48384}, \tfrac{1327}{4032}, 0, 0, -\tfrac{3}{32}, -\tfrac{1355}{6912}, -\tfrac{4385}{6912}]\ \theta_4,\\
B_5^6 &= \phi_5(y) + [-\tfrac{25}{14976}, \tfrac{25}{14976}, \tfrac{25}{14976}, 0, \tfrac{337}{4992}, \tfrac{1}{16}, \tfrac{35}{4992}, -\tfrac{235}{768}, -\tfrac{18025}{59904}, \tfrac{275}{832}, 0, -\tfrac{329}{1664}, -\tfrac{7}{32}, \tfrac{665}{7488}, -\tfrac{106435}{29952}]\ \theta_4.
\end{aligned}
$$

By Theorem 3.1, to locate the superconvergent points of the Poisson equation, we may choose B_{n+1}^j as ψs. Then we can verify the following results for n up to 8.

Proposition 3.3. *Consider element $\hat{T}_1$ of the Chevron mesh. For the Poisson equation, the function value superconvergent points are:*
(i) If n is odd, there is no superconvergent point;
(ii) If n is even, the midpoints of sides l_{12} and l_{15} are the only superconvergent points.

Proposition 3.4. *Consider element $\hat{T}_1$ of the Chevron mesh. For the Poisson equation, the x-derivative superconvergent points are:*
(i) If n is odd, the midpoint of side l_{12} is the only superconvergent point;
(ii) If n is even, there is no superconvergent point.
The y-derivative superconvergent points are:
(i) If $n = 1$, the midpoint of side l_{25} is the only superconvergent point;
(ii) If $n > 1$, there is no superconvergent point.

Remark 3.7. Similar as in the regular pattern, superconvergence for the Chevron pattern at symmetry points can be shown by symmetric properties of periodic basis functions and Legendre polynomials. However, Propositions 3.3 and 3.4 are conclusive. Moreover, the result of y-derivative superconvergence for $n = 1$ is not at a symmetry point. □

Remark 3.8. The basis functions of $\Phi_{n+1}(\hat{K})$ obtained from the orthogonal decomposition reveal the structures. However, there are more elements involved in the Chevron pattern than in the regular pattern, and the expressions of the basis functions here are even more complicated. Thus, we may use the second approach: solving a periodic finite element approximation problem. □

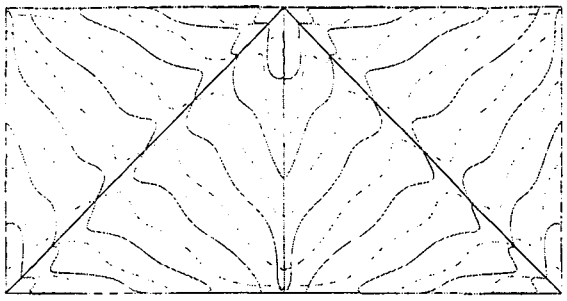

Figure 8: Contours $\psi_9^{Re} = 0$ (solid) and $\psi_9^{Im} = 0$ (dashed).

Next, we turn to harmonic polynomials (for the Laplace equation). With the help of basis functions of $\Phi_{n+1}(\hat{K})$, we can determine ψ_{n+1}^{Re} and ψ_{n+1}^{Im}. In particular, in the element $\hat{T}_1$, we have, for instance

$$\psi_2^{Re} = B_2^1 - B_2^3 = x^2 - y^2 + x + y,$$
$$\psi_2^{Im} = B_2^2 = xy;$$

$$\psi_3^{Re} = B_3^1 - 3B_3^3 = x^3 - 3xy^2 + \tfrac{3}{2}x^2 + \tfrac{3}{2}xy + \tfrac{1}{2}x,$$
$$\psi_3^{Im} = B_3^4 - 3B_3^2 = y^3 - 3x^2y - \tfrac{3}{2}y^2 - \tfrac{3}{2}xy + \tfrac{1}{2}y;$$

$$\psi_4^{Re} = B_4^1 - 6B_4^3 + B_4^5 = x^4 - 6x^2y^2 + y^4 + 2x^3 + 3x^2y - 3xy^2 - 2y^3 + x^2 + 2xy + y^2 - \tfrac{1}{30},$$
$$\psi_4^{Im} = B_4^2 - B_4^4 = x^3y - xy^3 + x^2y + xy^2;$$

$$\begin{aligned}\psi_5^{Re} &= B_5^1 - 10B_5^3 + 5B_5^5 \\ &= x^5 - 10x^3y^2 + 5xy^4 + \tfrac{5}{2}x^4 + \tfrac{85}{24}x^3y - \tfrac{35}{4}x^2y^2 - \tfrac{175}{24}xy^3 + \tfrac{85}{42}x^3 + \tfrac{15}{4}x^2y + \tfrac{10}{7}xy^2 + \tfrac{15}{28}x^2 + \tfrac{15}{28}xy + \tfrac{1}{84}x,\end{aligned}$$
$$\begin{aligned}\psi_5^{Im} &= B_5^6 - 10B_5^4 + 5B_5^2 \\ &= y^5 - 10y^3x^2 + 5yx^4 - \tfrac{5}{2}y^4 - \tfrac{85}{24}xy^3 + \tfrac{35}{4}x^2y^2 + \tfrac{175}{24}x^3y + \tfrac{85}{42}y^3 + \tfrac{15}{4}xy^2 + \tfrac{10}{7}x^2y - \tfrac{15}{28}y^2 - \tfrac{15}{28}xy + \tfrac{1}{84}y.\end{aligned}$$

For information of $n = 5, \ldots, 8$, the reader is referred to [13].

Now, we are ready to apply Theorem 3.2. The superconvergent points can be located by solving the corresponding systems. These can be done as for the regular pattern. However, the affine mapping from $\hat{T}_1^{Ch}$ to $\hat{T}_1^{Rg}$ ($x^{Rg} = 2x^{Ch} + 1$, $y^{Rg} = 2y^{Ch} - 1$) simplifies our life. When $n > 1$, under this mapping, $(\psi_{n+1}^{Re}|_{\hat{T}_1})^{Ch}$ and $(\psi_{n+1}^{Im}|_{\hat{T}_1})^{Ch}$ are the same as $(\psi_{n+1}^{Re}|_{\hat{T}_1})^{Rg}$ and $(\psi_{n+1}^{Im}|_{\hat{T}_1})^{Rg}$ up to a constant multiplier. When $n = 1$, they are the same up to a constant multiplier and a constant addendum as well.

Therefore, when $n > 1$, the function value and derivative superconvergent points in $\hat{T}_1^{Ch}$ can be obtained from those in $\hat{T}_1^{Rg}$ (see Remark 3.5), which are listed in TABLE 1 and TABLE 2. When $n = 1$, the derivative superconvergent points are also obtained from the regular pattern (TABLE 2). We need to determine only the function value superconvergent points, which are solutions of

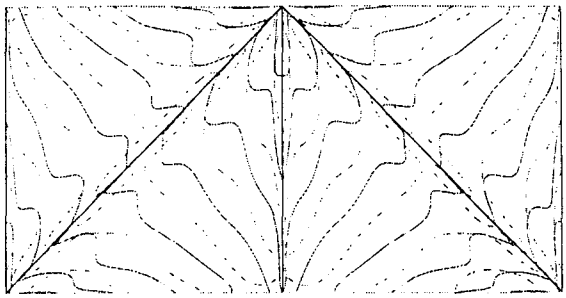

Figure 9: Contours $\frac{\partial \psi_9^{Re}}{\partial x} = 0$ (solid) and $\frac{\partial \psi_9^{Im}}{\partial x} = 0$ (dashed).

$$\begin{cases} x^2 - y^2 + x + y = 0, \\ xy = 0. \end{cases}$$

Solving this system, we have three superconvergent points: $(0,0)$, $(0,1)$ and $(-1,0)$. The contours $\psi_{n+1}^{Re} = 0$ and $\psi_{n+1}^{Im} = 0$ for $n = 8$ are given in FIGURE 8. The contours $\frac{\partial \psi_{n+1}^{Re}}{\partial x} = 0$ and $\frac{\partial \psi_{n+1}^{Im}}{\partial x} = 0$ for $n = 8$ are given in FIGURE 9.

3.3. UNION JACK PATTERN

In the Union Jack pattern, the reference cell is again $\hat{K} = [-1,1]^2$, which is partitioned into eight triangular elements (see FIGURE 10).

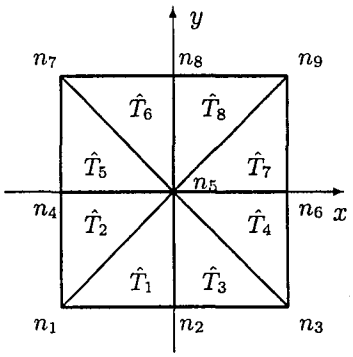

Figure 10: Partition of $\hat{K}$ for the Union Jack Pattern

Let ν_i be the linear nodal shape function corresponding to vertex n_i, which are defined in (3.23). The nodal shape functions are symmetric corresponding to the geometry of the vertices. The side modes and internal modes are defined as in (3.6) and (3.7), respectively.

The constructions of the periodic basis functions are similar as described in Section 3.1. Here, $\nu_1 + \nu_3 + \nu_7 + \nu_9$, $\nu_2 + \nu_8$, $\nu_4 + \nu_6$ and ν_5 are four periodic basis functions.

$$\nu_1 = \begin{cases} -x & \text{in } \hat{T}_1, \\ -y & \text{in } \hat{T}_2, \\ 0 & \text{in other } \hat{T}_i; \end{cases} \qquad \nu_2 = \begin{cases} x-y & \text{in } \hat{T}_1, \\ -x-y & \text{in } \hat{T}_3, \\ 0 & \text{in other } \hat{T}_i; \end{cases}$$

$$\nu_3 = \begin{cases} x & \text{in } \hat{T}_3, \\ -y & \text{in } \hat{T}_4, \\ 0 & \text{in other } \hat{T}_i; \end{cases} \qquad \nu_4 = \begin{cases} -x+y & \text{in } \hat{T}_2, \\ -x-y & \text{in } \hat{T}_5, \\ 0 & \text{in other } \hat{T}_i; \end{cases}$$

$$\nu_5 = \begin{cases} 1+y & \text{in } \hat{T}_1,\ \hat{T}_3, \\ 1+x & \text{in } \hat{T}_2,\ \hat{T}_5, \\ 1-x & \text{in } \hat{T}_4,\ \hat{T}_7, \\ 1-y & \text{in } \hat{T}_6,\ \hat{T}_8; \end{cases} \qquad \nu_6 = \begin{cases} x+y & \text{in } \hat{T}_4, \\ x-y & \text{in } \hat{T}_7, \\ 0 & \text{in other } \hat{T}_i; \end{cases} \tag{3.23}$$

$$\nu_7 = \begin{cases} y & \text{in } \hat{T}_5, \\ -x & \text{in } \hat{T}_6, \\ 0 & \text{in other } \hat{T}_i; \end{cases} \qquad \nu_8 = \begin{cases} x+y & \text{in } \hat{T}_6, \\ -x+y & \text{in } \hat{T}_8, \\ 0 & \text{in other } \hat{T}_i; \end{cases}$$

$$\nu_9 = \begin{cases} y & \text{in } \hat{T}_7, \\ x & \text{in } \hat{T}_8, \\ 0 & \text{in other } \hat{T}_i. \end{cases}$$

It is straightforward to verify that

$$\dim P_n^w(\hat{K}) = (2n+1)^2, \quad \dim PP_n^w(\hat{K}) = (2n)^2. \tag{3.24}$$

Theorems 3.1 and 3.2 are valid for the Union Jack mesh. To determine spaces $\Phi_{n+1}(\hat{K})$, we may either process an orthogonal decomposition of $PP_n^w(\hat{K})$ under the Laplace operator, or carry on a periodic finite element approximation. The first approach is similar as in previous cases. We define $\Psi_n(\hat{K})$ as in (3.11). Then by the Gram-Schmidt process, $PP_n^w(\hat{K})$ can be decomposed into a sum of $\Psi_n(\hat{K})$, as in (3.12). Based on $\Psi_n(\hat{K})$, we can construct $\Phi_n(\hat{K})$. [4]

Remark 3.9. For the Union Jack pattern, a portion of $\hat{K}$ in each quadrant can be mapped to the reference cell of the regular pattern by an affine mapping. The corresponding shape functions defined in (3.23) are mapped to the ones of the regular pattern. Similar symmetry results as in Lemma 3.3 hold for the Union Jack pattern. Therefore, we need to work only on superconvergent points in the first element. Superconvergent points in the other elements can be obtained by symmetry. □

Basis functions of $\Phi_{n+1}(\hat{K})$ in $\hat{T}_1$ are provided for $n = 1, \ldots, 4$. For information of $n = 5, \ldots, 8$, the reader is referred to [13]. To simplify notations, let B_{n+1}^j and θ_n be as defined in Section 3.2. Thus, the basis functions of $\Phi_{n+1}(\hat{K})$ in $\hat{T}_1$ are

$B_2^1 = \phi_2(x) + [\frac{7}{36}, \frac{11}{18}, \frac{25}{36}]\ \theta_1,$
$B_2^2 = xy + [-1, 0, 0]\ \theta_1,$
$B_2^3 = \phi_2(y) + [\frac{25}{36}, \frac{11}{18}, \frac{43}{36}]\ \theta_1;$

[4] As described in Remarks 3.3, 3.8, the second approach is more efficient in case that we are interested only in the expression itself (not the structure of the expression).

$$
\begin{aligned}
B_3^1 &= \phi_3(x) + [-\tfrac{3}{40}, 0, 0, \tfrac{27}{80}, 0, \tfrac{3}{8}]\ \theta_2,\\
B_3^2 &= \phi_2(x)y + [\tfrac{11}{40}, 0, \tfrac{11}{20}, \tfrac{1}{4}, \tfrac{1}{80}, \tfrac{3}{8}]\ \theta_2,\\
B_3^3 &= x\phi_2(y) + [-\tfrac{31}{40}, 0, 0, -\tfrac{1}{80}, 0, \tfrac{3}{8}]\ \theta_2,\\
B_3^4 &= \phi_3(y) + [\tfrac{3}{40}, 0, \tfrac{33}{20}, 0, \tfrac{33}{80}, \tfrac{3}{8}]\ \theta_2;
\end{aligned}
$$

$$
\begin{aligned}
B_4^1 &= \phi_4(x) + [\tfrac{1}{56}, -\tfrac{13}{112}, \tfrac{3}{56}, -\tfrac{33}{224}, \tfrac{15}{224}, -\tfrac{3}{112}, \tfrac{31}{112}, \tfrac{1}{112}, \tfrac{5}{16}, -\tfrac{15}{14}]\ \theta_3,\\
B_4^2 &= \phi_3(x)y + [-\tfrac{19}{140}, 0, 0, -\tfrac{1}{7}, 0, \tfrac{19}{280}, \tfrac{1}{8}, 0, \tfrac{1}{4}, -\tfrac{5}{7}]\ \theta_3,\\
B_4^3 &= \phi_2(x)\phi_2(y) + [\tfrac{439}{5040}, -\tfrac{1247}{5040}, \tfrac{319}{5040}, \tfrac{65}{336}, \tfrac{25}{168}, \tfrac{61}{168}, -\tfrac{1}{336}, \tfrac{1}{336}, \tfrac{1}{8}, -\tfrac{17}{168}]\ \theta_3,\\
B_4^4 &= x\phi_3(y) + [-\tfrac{19}{140}, 0, 0, -\tfrac{1}{56}, 0, \tfrac{229}{280}, 0, 0, \tfrac{1}{4}, \tfrac{15}{28}]\ \theta_3,\\
B_4^5 &= \phi_4(y) + [-\tfrac{3}{28}, -\tfrac{13}{112}, \tfrac{13}{4}, -\tfrac{3}{224}, \tfrac{429}{224}, \tfrac{207}{112}, -\tfrac{1}{112}, \tfrac{39}{112}, \tfrac{5}{16}, \tfrac{10}{7}]\ \theta_3;
\end{aligned}
$$

$$
\begin{aligned}
B_5^1 &= \phi_5(x) + [-\tfrac{115}{5184}, 0, 0, -\tfrac{2215}{27648}, 0, -\tfrac{289}{13824}, -\tfrac{23245}{82944}, 0, -\tfrac{9275}{41472}, -\tfrac{15665}{41472}, \tfrac{2065}{10368}, 0, \tfrac{7}{32}, -\tfrac{8155}{2304}, -\tfrac{35}{5184}]\ \theta_4,\\
B_5^2 &= \phi_4(x)y + [\tfrac{305}{4032}, 0, -\tfrac{269}{4032}, \tfrac{1991}{21504}, \tfrac{1}{28}, \tfrac{37}{1536}, -\tfrac{295}{3072}, \tfrac{55}{5376}, \tfrac{173}{32256}, -\tfrac{12331}{32256}, \tfrac{1}{16}, \tfrac{1}{1152}, \tfrac{5}{32}, -\tfrac{995}{576}, -\tfrac{445}{2304}]\ \theta_4,\\
B_5^3 &= \phi_3(x)\phi_2(y) + [-\tfrac{137}{2268}, 0, 0, -\tfrac{120137}{483840}, 0, -\tfrac{8623}{48384}, \tfrac{30089}{290304}, 0, \tfrac{23755}{145152}, -\tfrac{53411}{145152}, -\tfrac{19}{25920}, 0, \tfrac{1}{16}, -\tfrac{275}{1152}, -\tfrac{383}{2592}]\ \theta_4,\\
B_5^4 &= \phi_2(x)\phi_3(y) + [\tfrac{137}{2268}, 0, \tfrac{863}{18144}, \tfrac{1307}{32256}, \tfrac{2917}{13440}, \tfrac{41}{256}, -\tfrac{107}{41472}, \tfrac{2579}{36288}, \tfrac{41899}{145152}, -\tfrac{5585}{145152}, 0, \tfrac{19}{25920}, \tfrac{1}{16}, \tfrac{427}{2592}, -\tfrac{59}{1152}]\ \theta_4,\\
B_5^5 &= x\phi_4(y) + [\tfrac{199}{4032}, 0, 0, -\tfrac{61}{7168}, 0, \tfrac{3837}{3584}, -\tfrac{95}{21504}, 0, \tfrac{30413}{32256}, \tfrac{51391}{32256}, -\tfrac{1}{1152}, 0, \tfrac{5}{32}, \tfrac{995}{2304}, \tfrac{715}{576}]\ \theta_4,\\
B_5^6 &= \phi_5(y) + [\tfrac{115}{5184}, 0, \tfrac{34055}{5184}, \tfrac{5}{9216}, \tfrac{2017}{384}, \tfrac{7859}{1536}, -\tfrac{875}{82944}, \tfrac{43075}{20736}, \tfrac{81445}{41472}, \tfrac{268645}{41472}, 0, \tfrac{2471}{10368}, \tfrac{7}{32}, -\tfrac{35}{5184}, \tfrac{9485}{2304}]\ \theta_4.
\end{aligned}
$$

Choose B_{n+1}^j as ψs, apply Theorem 3.1, and we can verify the following results for finite elements of degree n up to 8.

Proposition 3.5. *Consider element $\hat{T}_1$ of the Union Jack mesh. For the Poisson equation, the function value superconvergent points are:*
(i) If n is odd, there is no superconvergent point;
(ii) If n is even, the vertices and the midpoint of side l_{15} are the only superconvergent points.

Proposition 3.6. *Consider element $\hat{T}_1$ of the Union Jack mesh. For the Poisson equation, there is no superconvergent point for $\frac{\partial u}{\partial x}$, nor for $\frac{\partial u}{\partial y}$.*

Remark 3.10. Propositions 3.5 and 3.6 agree with the results from the computer-based proof and the conclusion from the symmetry principle. Moreover, our results theoretically confirmed that there are no other superconvergent points. □

Now, we consider harmonic polynomials. Again, we can determine ψ_{n+1}^{Re} and ψ_{n+1}^{Im} from the basis functions of $\Phi_{n+1}(\hat{K})$. In the element $\hat{T}_1$, we have, for instance

$$
\begin{aligned}
\psi_2^{Re} &= B_2^1 - B_2^3 = x^2 - y^2 + x - y,\\
\psi_2^{Im} &= B_2^2 = xy + x;
\end{aligned}
$$

$$
\begin{aligned}
\psi_3^{Re} &= B_3^1 - 3B_3^3 = x^3 - 3xy^2 + \tfrac{3}{2}x^2 - \tfrac{9}{2}xy - x,\\
\psi_3^{Im} &= B_3^4 - 3B_3^2 = y^3 - 3x^2y + \tfrac{3}{2}y^2 - \tfrac{3}{2}xy - 3x^2 + \tfrac{1}{2}y - \tfrac{3}{2}x;
\end{aligned}
$$

$$
\begin{aligned}
\psi_4^{Re} &= B_4^1 - 6B_4^3 + B_4^5 = x^4 - 6x^2y^2 + y^4 + 2x^3 - 9x^2y - 3xy^2 + 2y^3 - 2x^2 - 4xy + y^2 - x - \tfrac{1}{30},\\
\psi_4^{Im} &= B_4^2 - B_4^4 = x^3y - xy^3 + x^3 + x^2y - 2xy^2 + x^2 - xy;
\end{aligned}
$$

$$
\begin{aligned}
\psi_5^{Re} &= B_5^1 - 10B_5^3 + 5B_5^5 = x^5 - 10x^3y^2 + 5xy^4 + \tfrac{5}{2}x^4 - \tfrac{395}{24}x^3y - \tfrac{35}{4}x^2y^2 + \tfrac{305}{24}xy^3\\
&\quad - \tfrac{745}{168}x^3 - \tfrac{55}{4}x^2y + \tfrac{535}{56}xy^2 - \tfrac{125}{28}x^2 + \tfrac{85}{56}xy - \tfrac{53}{168}x,\\
\psi_5^{Im} &= B_5^6 - 10B_5^4 + 5B_5^2 = y^5 - 10x^2y^3 + 5x^4y + \tfrac{5}{2}y^4 - \tfrac{85}{24}xy^3 - \tfrac{85}{4}x^2y^2 + \tfrac{175}{24}x^3y\\
&\quad + 5x^4 + \tfrac{85}{42}y^3 - \tfrac{55}{8}xy^2 - \tfrac{155}{14}x^2y + \tfrac{175}{24}x^3 + \tfrac{15}{28}y^2 - \tfrac{205}{56}xy + \tfrac{5}{28}x^2 + \tfrac{1}{84}y - \tfrac{55}{168}x.
\end{aligned}
$$

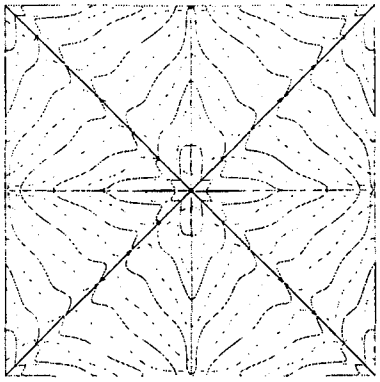

Figure 11: Contours $\psi_9^{Re} = 0$ (solid) and $\psi_9^{Im} = 0$ (dashed).

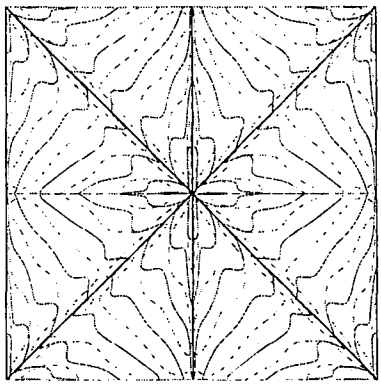

Figure 12: Contours $\frac{\partial \psi_9^{Re}}{\partial x} = 0$ (solid) and $\frac{\partial \psi_9^{Im}}{\partial x} = 0$ (dashed).

For information of more cases, please check [13].

By Theorem 3.2, The superconvergent points can be located by solving the corresponding systems. These can be done as for the regular pattern. However, as we observed for the Chevron patter, the affine mapping from $\hat{T}_1^{UJ}$ to $\hat{T}_1^{Rg}$ maps $(\psi_{n+1}^{Re}|_{\hat{T}_1})^{UJ}$ and $(\psi_{n+1}^{Im}|_{\hat{T}_1})^{UJ}$ to $(\psi_{n+1}^{Re}|_{\hat{T}_1})^{Rg}$ and $(\psi_{n+1}^{Im}|_{\hat{T}_1})^{Rg}$ up to a constant multiplier when $n > 1$. When $n = 1$, they coincide with each other up to a constant multiplier and a constant addendum as well.

Thus, when $n > 1$, the function value and derivative superconvergent points in $\hat{T}_1^{UJ}$ can be obtained from those in $\hat{T}_1^{Rg}$, which are listed in TABLE 1 and TABLE 2. When $n = 1$, the derivative superconvergent points are also as same as the regular pattern (TABLE 2). Therefore, we need to determine only the function value superconvergent points for $n = 1$. Toward this end, we solve

$$\begin{cases} x^2 - y^2 + x - y = 0, \\ xy + x = 0, \end{cases}$$

and find three superconvergent points: $(0,0)$, $(0,-1)$ and $(-1,-1)$. The contours $\psi_{n+1}^{Re} = 0$ and $\psi_{n+1}^{Im} = 0$ for $n = 8$ are given in FIGURE 11. The contours $\frac{\partial \psi_{n+1}^{Re}}{\partial x} = 0$ and $\frac{\partial \psi_{n+1}^{Im}}{\partial x} = 0$

for $n = 8$ are given in FIGURE 12.

3.4. CRISS-CROSS PATTERN

In the Criss-Cross Pattern, we partition the reference cell $\hat{K} = [-1, 1]^2$ into four triangular elements (see FIGURE 13).

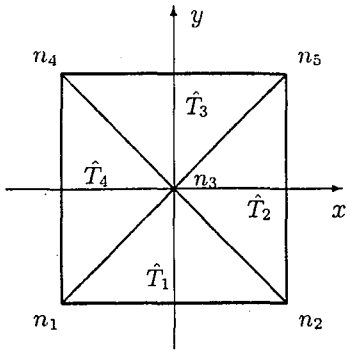

Figure 13: Partition of $\hat{K}$ for the Criss-Cross Pattern

Let ν_i be the linear nodal shape function corresponding to vertex n_i.

$$\nu_1 = \begin{cases} -\frac{1}{2}(x+y) & \text{in } \hat{T}_1,\ \hat{T}_4, \\ 0 & \text{in } \hat{T}_2,\ \hat{T}_3; \end{cases} \qquad \nu_2 = \begin{cases} \frac{1}{2}(x-y) & \text{in } \hat{T}_1,\ \hat{T}_2, \\ 0 & \text{in } \hat{T}_3,\ \hat{T}_4; \end{cases}$$

$$\nu_3 = \begin{cases} 1+y & \text{in } \hat{T}_1, \\ 1-x & \text{in } \hat{T}_2, \\ 1-y & \text{in } \hat{T}_3, \\ 1+x & \text{in } \hat{T}_4; \end{cases} \qquad \nu_4 = \begin{cases} \frac{1}{2}(y-x) & \text{in } \hat{T}_3,\ \hat{T}_4, \\ 0 & \text{in } \hat{T}_1,\ \hat{T}_2; \end{cases} \qquad \nu_5 = \begin{cases} \frac{1}{2}(x+y) & \text{in } \hat{T}_2,\ \hat{T}_3, \\ 0 & \text{in } \hat{T}_1,\ \hat{T}_4. \end{cases} \tag{3.25}$$

The side modes and internal modes are defined as in (3.6) and (3.7), respectively.

The periodic basis functions can be constructed from the hierarchic basis functions. This time, $\nu_1 + \nu_2 + \nu_4 + \nu_5$ and ν_3 are periodic.

It is straightforward to verify that

$$\dim P_n^w(\hat{K}) = n^2 + (n+1)^2, \quad \dim PP_n^w(\hat{K}) = 2n^2. \tag{3.26}$$

Again, Theorems 3.1 and 3.2 are valid for Criss-Cross mesh. To determine spaces $\Phi_{n+1}(\hat{K})$, we may either process the orthogonal decomposition of $PP_n^w(\hat{K})$, or carry on a periodic finite element approximation. As we mentioned before, the second approach is more efficient when we are interested only in the expressions (rather than the structures) of the basis functions.

Remark 3.11. Unlike the Chevron and Union Jack patterns, no portion of the partitioned $\hat{K}$ for the Criss-Cross pattern "looks like" the regular pattern. In other words, $\hat{T}_1$ and $\hat{T}_2$ can not be mapped to the reference cell of the regular pattern by an affine mapping, nor

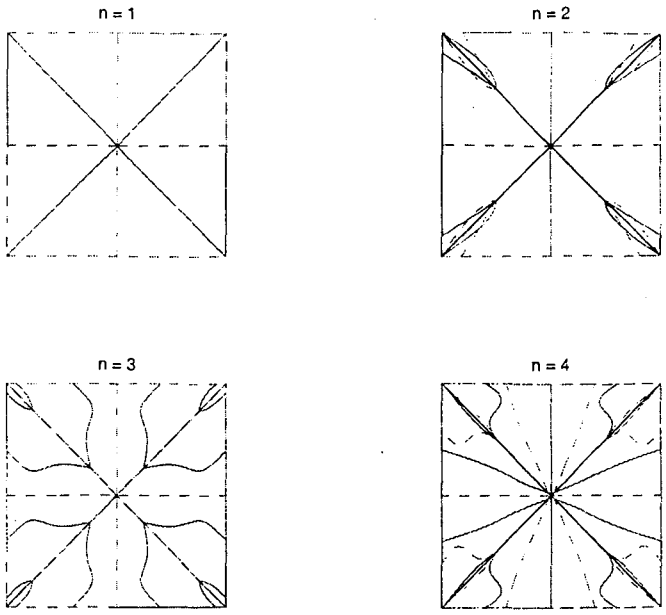

Figure 14: Contours $\psi_{n+1}^{Re} = 0$ (solid) and $\psi_{n+1}^{Im} = 0$ (dashed), $n = 1, \ldots, 4$.

can the other pairs. This leads to the fact that the superconvergence of the Criss-Cross pattern is very much different from that of the regular pattern.

On the other hand, the geometry of the partition in $\hat{K}$ is symmetric, as we can see in definition (3.25). So we need to study only superconvergence in $\hat{T}_1$ and $\hat{T}_2$. Superconvergent points in the other elements can be obtained by symmetry. □

In the following, basis functions of $\Phi_{n+1}(\hat{K})$ in $\hat{T}_1$ and $\hat{T}_2$ are provided for $n = 1, \ldots, 4$. For cases $n = 5, \ldots, 8$, the reader is referred to [13]. As in Section 3.2, we use B_{n+1}^j to denote the j^{th} basis function of $\Phi_{n+1}(\hat{K})$, and let column vectors θ_n^1 and θ_n^2 consist all nodal shape functions, side modes, and internal modes of order $\leq n$ in $\hat{T}_1$ and $\hat{T}_2$, respectively. For example,

$$\begin{aligned}
\theta_1^1 &= [\nu_1, \nu_2, \nu_3]^T, & \theta_1^2 &= [\nu_2, \nu_5, \nu_3]^T; \\
\theta_2^1 &= [\theta_1^1, \ \varsigma_2^{12}, \varsigma_2^{23}, \varsigma_2^{13}]^T, & \theta_2^2 &= [\theta_1^2, \ \varsigma_2^{25}, \varsigma_2^{35}, \varsigma_2^{23}]^T; \\
\theta_3^1 &= [\theta_2^1, \ \varsigma_3^{12}, \varsigma_3^{23}, \varsigma_3^{13}, \iota_{3,1}^1]^T, & \theta_3^2 &= [\theta_2^2, \ \varsigma_3^{25}, \varsigma_3^{35}, \varsigma_3^{23}, \iota_{3,1}^2]^T; \\
\theta_4^1 &= [\theta_3^1, \ \varsigma_4^{12}, \varsigma_4^{23}, \varsigma_4^{13}, \iota_{4,1}^1, \iota_{4,2}^1]^T, & \theta_4^2 &= [\theta_3^2, \ \varsigma_4^{25}, \varsigma_4^{35}, \varsigma_4^{23}, \iota_{4,1}^2, \iota_{4,2}^2]^T.
\end{aligned} \tag{3.27}$$

Then, in element $\hat{T}_1$, the basis functions of $\Phi_{n+1}(\hat{K})$ are

$$\begin{aligned}
B_2^1 &= \phi_2(x) + [\tfrac{2}{9}, \tfrac{2}{9}, \tfrac{5}{9}]\ \theta_1^1, \\
B_2^2 &= xy + [-1, 1, 0]\ \theta_1^1, \\
B_2^3 &= \phi_2(y) + [\tfrac{2}{9}, \tfrac{2}{9}, \tfrac{5}{9}]\ \theta_1^1;
\end{aligned}$$

$$B_3^1 = \phi_3(x) + [0, 0, 0, 0, -\tfrac{3}{10}, \tfrac{3}{10}]\ \theta_2^1,$$

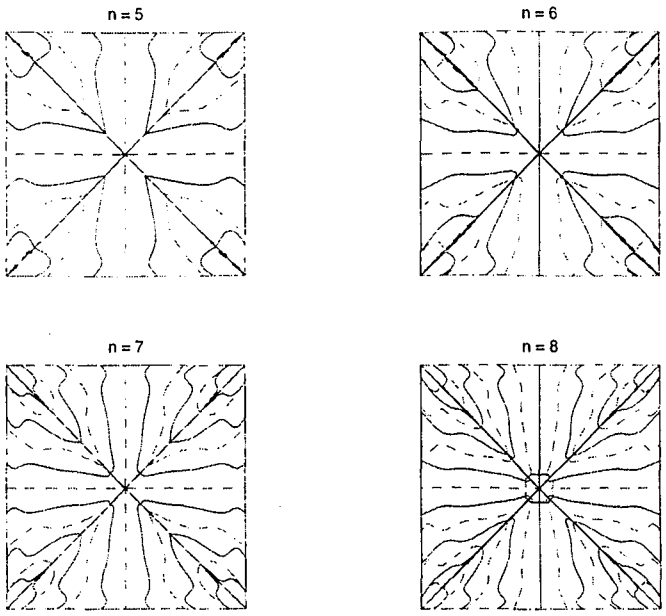

Figure 15: Contours $\psi_{n+1}^{Re} = 0$ (solid) and $\psi_{n+1}^{Im} = 0$ (dashed), $n = 5, \ldots, 8$.

$$B_3^2 = \phi_2(x)y + [0,0,0,1,\tfrac{7}{20},\tfrac{7}{20}]\ \theta_2^1,$$
$$B_3^3 = x\phi_2(y) + [0,0,0,0,-\tfrac{7}{20},\tfrac{7}{20}]\ \theta_2^1,$$
$$B_3^4 = \phi_3(y) + [0,0,0,0,\tfrac{3}{10},\tfrac{3}{10}]\ \theta_2^1;$$

$$B_4^1 = \phi_4(x) + [\tfrac{19}{336},\tfrac{19}{336},-\tfrac{5}{48},\tfrac{19}{112},-\tfrac{1}{14},-\tfrac{1}{14},0,\tfrac{25}{112},\tfrac{25}{112},-\tfrac{115}{56}]\ \theta_3^1,$$
$$B_4^2 = \phi_3(x)y + [0,0,0,0,\tfrac{1}{5},-\tfrac{1}{5},1,-\tfrac{8}{35},\tfrac{8}{35},0]\ \theta_3^1,$$
$$B_4^3 = \phi_2(x)\phi_2(y) + [\tfrac{1}{504},\tfrac{1}{504},-\tfrac{91}{360},\tfrac{1}{168},\tfrac{1}{42},\tfrac{1}{42},0,\tfrac{19}{168},\tfrac{19}{168},-\tfrac{97}{84}]\ \theta_3^1,$$
$$B_4^4 = x\phi_3(y) + [0,0,0,0,\tfrac{1}{5},-\tfrac{1}{5},0,-\tfrac{8}{35},\tfrac{8}{35},0]\ \theta_3^1,$$
$$B_4^5 = \phi_4(y) + [\tfrac{19}{336},\tfrac{19}{336},-\tfrac{5}{48},\tfrac{19}{112},-\tfrac{1}{14},-\tfrac{1}{14},0,\tfrac{25}{112},\tfrac{25}{112},\tfrac{125}{56}]\ \theta_3^1;$$

$$B_5^1 = \phi_5(x) + [0,0,0,0,\tfrac{121}{1728},-\tfrac{121}{1728},\tfrac{85}{864},\tfrac{145}{576},-\tfrac{145}{576},0,0,-\tfrac{217}{1296},\tfrac{217}{1296},-\tfrac{13895}{2592},0]\ \theta_4^1,$$
$$B_5^2 = \phi_4(x)y + [0,0,0,0,\tfrac{251}{4032},\tfrac{251}{4032},0,-\tfrac{1019}{4032},-\tfrac{1019}{4032},-\tfrac{2159}{3024},1,\tfrac{61}{432},\tfrac{61}{432},0,-\tfrac{2635}{864}]\ \theta_4^1,$$
$$B_5^3 = \phi_3(x)\phi_2(y) + [0,0,0,0,\tfrac{947}{7560},-\tfrac{947}{7560},\tfrac{1}{756},\tfrac{3}{56},-\tfrac{3}{56},0,0,-\tfrac{47}{810},\tfrac{47}{810},-\tfrac{509}{324},0]\ \theta_4^1,$$
$$B_5^4 = \phi_2(x)\phi_3(y) + [0,0,0,0,-\tfrac{947}{7560},-\tfrac{947}{7560},0,-\tfrac{3}{56},-\tfrac{3}{56},\tfrac{67}{1134},0,\tfrac{47}{810},\tfrac{47}{810},0,-\tfrac{373}{324}]\ \theta_4^1,$$
$$B_5^5 = x\phi_4(y) + [0,0,0,0,-\tfrac{251}{4032},\tfrac{251}{4032},\tfrac{5}{672},\tfrac{1019}{4032},-\tfrac{1019}{4032},0,0,-\tfrac{61}{432},\tfrac{61}{432},\tfrac{445}{864},0]\ \theta_4^1,$$
$$B_5^6 = \phi_5(y) + [0,0,0,0,-\tfrac{121}{1728},-\tfrac{121}{1728},0,-\tfrac{145}{576},-\tfrac{145}{576},\tfrac{2245}{1296},0,\tfrac{217}{1296},\tfrac{217}{1296},0,\tfrac{13265}{2592}]\ \theta_4^1.$$

In element $\hat{T}_2$, the basis functions of $\Phi_{n+1}(\hat{K})$ are

$$B_2^1 = \phi_2(x) + [\tfrac{2}{9},\tfrac{2}{9},\tfrac{5}{9}]\ \theta_1^2,$$
$$B_2^2 = xy + [1,-1,0]\ \theta_1^2,$$
$$B_2^3 = \phi_2(y) + [\tfrac{2}{9},\tfrac{2}{9},\tfrac{5}{9}]\ \theta_1^2;$$

$$B_3^1 = \phi_3(x) + [0,0,0,0,-\tfrac{3}{10},-\tfrac{3}{10}]\ \theta_2^2,$$
$$B_3^2 = \phi_2(x)y + [0,0,0,0,-\tfrac{7}{20},\tfrac{7}{20}]\ \theta_2^2,$$

$$B_3^3 = x\phi_2(y) + [0,0,0,-1,-\tfrac{7}{20},-\tfrac{7}{20}]\ \theta_2^2,$$
$$B_3^4 = \phi_3(y) + [0,0,0,0,-\tfrac{3}{10},\tfrac{3}{10}]\ \theta_2^2;$$

$$B_4^1 = \phi_4(x) + [\tfrac{19}{336},\tfrac{19}{336},-\tfrac{5}{48},\tfrac{19}{112},-\tfrac{1}{14},-\tfrac{1}{14},0,\tfrac{25}{112},\tfrac{25}{112},\tfrac{125}{56}]\ \theta_3^2,$$
$$B_4^2 = \phi_3(x)y + [0,0,0,0,-\tfrac{1}{5},\tfrac{1}{5},0,\tfrac{8}{35},-\tfrac{8}{35},0]\ \theta_3^2,$$
$$B_4^3 = \phi_2(x)\phi_2(y) + [\tfrac{1}{504},\tfrac{1}{504},-\tfrac{91}{360},\tfrac{1}{168},\tfrac{1}{42},\tfrac{1}{42},0,\tfrac{19}{168},\tfrac{19}{168},-\tfrac{97}{84}]\ \theta_3^2,$$
$$B_4^4 = x\phi_3(y) + [0,0,0,0,-\tfrac{1}{5},\tfrac{1}{5},-1,\tfrac{8}{35},-\tfrac{8}{35},0]\ \theta_3^2,$$
$$B_4^5 = \phi_4(y) + [\tfrac{19}{336},\tfrac{19}{336},-\tfrac{5}{48},\tfrac{19}{112},-\tfrac{1}{14},-\tfrac{1}{14},0,\tfrac{25}{112},\tfrac{25}{112},-\tfrac{115}{56}]\ \theta_3^2;$$

$$B_5^1 = \phi_5(x) + [0,0,0,0,\tfrac{121}{1728},\tfrac{121}{1728},0,\tfrac{145}{576},\tfrac{145}{576},-\tfrac{2245}{1296},0,-\tfrac{217}{1296},-\tfrac{217}{1296},\tfrac{13265}{2592},0]\ \theta_4^2,$$
$$B_5^2 = \phi_4(x)y + [0,0,0,0,-\tfrac{251}{4032},\tfrac{251}{4032},\tfrac{5}{672},\tfrac{1019}{4032},-\tfrac{1019}{4032},0,0,-\tfrac{61}{432},\tfrac{61}{432},0,\tfrac{445}{864}]\ \theta_4^2,$$
$$B_5^3 = \phi_3(x)\phi_2(y) + [0,0,0,0,\tfrac{947}{7560},\tfrac{947}{7560},0,\tfrac{3}{56},\tfrac{3}{56},-\tfrac{67}{1134},0,-\tfrac{47}{810},-\tfrac{47}{810},-\tfrac{373}{324},0]\ \theta_4^2,$$
$$B_5^4 = \phi_2(x)\phi_3(y) + [0,0,0,0,\tfrac{947}{7560},-\tfrac{947}{7560},\tfrac{1}{756},\tfrac{3}{56},-\tfrac{3}{56},0,0,-\tfrac{47}{810},\tfrac{47}{810},0,-\tfrac{509}{324}]\ \theta_4^2,$$
$$B_5^5 = x\phi_4(y) + [0,0,0,0,-\tfrac{251}{4032},-\tfrac{251}{4032},0,\tfrac{1019}{4032},\tfrac{1019}{4032},\tfrac{2159}{3024},-1,-\tfrac{61}{432},-\tfrac{61}{432},-\tfrac{2635}{864},0]\ \theta_4^2,$$
$$B_5^6 = \phi_5(y) + [0,0,0,0,\tfrac{121}{1728},-\tfrac{121}{1728},\tfrac{85}{864},\tfrac{145}{576},-\tfrac{145}{576},0,0,-\tfrac{217}{1296},\tfrac{217}{1296},0,-\tfrac{13895}{2592}]\ \theta_4^2.$$

Take B_{n+1}^j as ψs, and we can verify the following results for n up to 8.

Proposition 3.7. *Consider element $\hat{T}_1$ (or $\hat{T}_2$) of the Criss-Cross mesh. For the Poisson equation, the function value superconvergent points are:*
(i) If n is odd, there is no superconvergent point;
(ii) If n is even, the vertices and the midpoint of side l_{12} (or l_{25}, respectively) are the only superconvergent points.

Proposition 3.8. *Consider the superconvergent points for $\frac{\partial u}{\partial x}$ of the Poisson solutions in the Criss-Cross mesh. In $\hat{T}_1$, the superconvergent points are the same as in the regular pattern. In $\hat{T}_2$, there is no superconvergent point.*

For $\frac{\partial u}{\partial y}$, superconvergence can be determined by symmetry. Namely, in $\hat{T}_1$, there is no superconvergent point. In $\hat{T}_2$, the cases are the same as in the regular pattern.

Remark 3.12. As in the regular pattern, superconvergence for the Criss-Cross pattern at symmetry points was predicted by the symmetry theory and the computer-based proof. Propositions 3.7 and 3.8 confirm theoretically that there are no other superconvergent points. □

As for the Laplace equation, we determine ψ_{n+1}^{Re} and ψ_{n+1}^{Im} from the basis functions of $\Phi_{n+1}(\hat{K})$. In the element $\hat{T}_1$, we have

$$\psi_2^{Re} = B_2^1 - B_2^3 = x^2 - y^2,$$
$$\psi_2^{Im} = B_2^2 = xy + x;$$

$$\psi_3^{Re} = B_3^1 - 3B_3^3 = x^3 - 3xy^2 - 3xy - x,$$
$$\psi_3^{Im} = B_3^4 - 3B_3^2 = y^3 - 3x^2y - 3x^2 - y;$$

$$\psi_4^{Re} = B_4^1 - 6B_4^3 + B_4^5 = x^4 - 6x^2y^2 + y^4 - 9x^2y + y^3 - 4x^2 + \tfrac{2}{15},$$
$$\psi_4^{Im} = B_4^2 - B_4^4 = x^3y - xy^3 + x^3 - xy^2;$$

$$\psi_5^{Re} = B_5^1 - 10B_5^3 + 5B_5^5 = x^5 - 10x^3y^2 + 5xy^4 - \tfrac{95}{6}x^3y + \tfrac{35}{6}xy^3 - \tfrac{605}{84}x^3 - \tfrac{25}{28}xy^2 - \tfrac{15}{7}xy - \tfrac{1}{21}x,$$
$$\psi_5^{Im} = B_5^6 - 10B_5^4 + 5B_5^2 = y^5 - 10y^3x^2 + 5yx^4 + \tfrac{5}{4}y^4 - \tfrac{65}{4}y^2x^2 + 5x^4 + \tfrac{25}{84}y^3 - \tfrac{235}{28}yx^2 - \tfrac{15}{7}x^2 - \tfrac{1}{21}y.$$

In the element $\hat{T}_2$, we have

$$\psi_2^{Re} = B_2^1 - B_2^3 = x^2 - y^2,$$
$$\psi_2^{Im} = B_2^2 = xy - y;$$

$$\psi_3^{Re} = B_3^1 - 3B_3^3 = x^3 - 3xy^2 + 3y^2 - x,$$
$$\psi_3^{Im} = B_3^4 - 3B_3^2 = y^3 - 3yx^2 + 3yx - y;$$

$$\psi_4^{Re} = B_4^1 - 6B_4^3 + B_4^5 = x^4 - 6x^2y^2 + y^4 - x^3 + 9xy^2 - 4y^2 + \tfrac{2}{15},$$
$$\psi_4^{Im} = B_4^2 - B_4^4 = x^3y - xy^3 - x^2y + y^3;$$

$$\psi_5^{Re} = B_5^1 - 10B_5^3 + 5B_5^5 = x^5 - 10x^3y^2 + 5xy^4 - \tfrac{5}{4}x^4 + \tfrac{65}{4}x^2y^2 - 5y^4 + \tfrac{25}{84}x^3 - \tfrac{235}{28}xy^2 + \tfrac{15}{7}y^2 - \tfrac{1}{21}x,$$
$$\psi_5^{Im} = B_5^6 - 10B_5^4 + 5B_5^2 = y^5 - 10y^3x^2 + 5yx^4 + \tfrac{95}{6}y^3x - \tfrac{35}{6}yx^3 - \tfrac{605}{84}y^3 - \tfrac{25}{28}yx^2 + \tfrac{15}{7}yx - \tfrac{1}{21}y.$$

For cases $n = 5, \ldots, 8$, the reader is referred to [13].

By Theorem 3.2, the intersection points of the contours $\psi_{n+1}^{Re} = 0$ and $\psi_{n+1}^{Im} = 0$ are function value superconvergent points. It can be shown that, for $k = 1, 2, \ldots$

$$\begin{aligned} \psi_{2k}^{Re}|_{\hat{T}_1}(-y,-x) &= (-1)^k \psi_{2k}^{Re}|_{\hat{T}_2}(x,y), \\ \psi_{2k}^{Im}|_{\hat{T}_1}(-y,-x) &= (-1)^{k+1} \psi_{2k}^{Im}|_{\hat{T}_2}(x,y); \\ \psi_{2k+1}^{Re}|_{\hat{T}_1}(-y,-x) &= -\psi_{2k+1}^{Im}|_{\hat{T}_2}(x,y), \\ \psi_{2k+1}^{Im}|_{\hat{T}_1}(-y,-x) &= -\psi_{2k+1}^{Re}|_{\hat{T}_2}(x,y). \end{aligned} \tag{3.28}$$

TABLE 3(a). Function Value Superconvergent Points for the Criss-Cross Pattern (in $\hat{T}_1$, $n = 1, \ldots, 4$)

	$n=1$	$n=2$	$n=3$	$n=4$
1	−1.0000000000000000 −1.0000000000000000	−1.0000000000000000 −1.0000000000000000	−0.9173685331054181 −1.0000000000000000	−1.0000000000000000 −1.0000000000000000
2	1.0000000000000000 −1.0000000000000000	0.0000000000000000 −1.0000000000000000	−0.3980389107461900 −1.0000000000000000	−0.6074928962939559 −1.0000000000000000
3	0.0000000000000000 0.0000000000000000	1.0000000000000000 −1.0000000000000000	0.3980389107461900 −1.0000000000000000	0.0000000000000000 −1.0000000000000000
4		−0.6614378277661476 −0.7500000000000000	0.9173685331054181 −1.0000000000000000	0.6074928962939559 −1.0000000000000000
5		0.6614378277661476 −0.7500000000000000	−0.7596648111796141 −0.7596648111796141	1.0000000000000000 −1.0000000000000000
6		−0.5000000000000000 −0.5000000000000000	0.7596648111796141 −0.7596648111796141	−0.9755948656056709 −0.9755948656056709
7		0.5000000000000000 −0.5000000000000000	−0.2403351888203859 −0.2403351888203859	0.9755948656056709 −0.9755948656056709
8		0.0000000000000000 0.0000000000000000	0.2403351888203859 −0.2403351888203859	−0.5266244945254620 −0.5437574858837224
9				0.5266244945254620 −0.5437574858837224
10				−0.5000000000000000 −0.5000000000000000
11				0.5000000000000000 −0.5000000000000000
12				−0.0244051343943291 −0.0244051343943291
13				0.0244051343943291 −0.0244051343943291
14				0.0000000000000000 0.0000000000000000

TABLE 3(b). Function Value Superconvergent Points for the Criss-Cross Pattern (in $\hat{T}_1$, $n = 5, \ldots, 8$)

	$n = 5$	$n = 6$	$n = 7$	$n = 8$
1	−1.0000000000000000 −1.0000000000000000	−1.0000000000000000 −1.0000000000000000	−0.9981396004694932 −1.0000000000000000	−1.0000000000000000 −1.0000000000000000
2	−0.7520955703220618 −1.0000000000000000	−0.8258100260262924 −1.0000000000000000	−0.8677139861534285 −1.0000000000000000	−0.8949872464334571 −1.0000000000000000
3	−0.2738197456392299 −1.0000000000000000	−0.4616469028358420 −1.0000000000000000	−0.5861275452213199 −1.0000000000000000	−0.6718072968265310 −1.0000000000000000
4	0.2738197456392299 −1.0000000000000000	0.0000000000000000 −1.0000000000000000	−0.2065452580134060 −1.0000000000000000	−0.3593519628863694 −1.0000000000000000
5	0.7520955703220618 −1.0000000000000000	0.4616469028358420 −1.0000000000000000	0.2065452580134060 −1.0000000000000000	0.0000000000000000 −1.0000000000000000
6	1.0000000000000000 −1.0000000000000000	0.8258100260262924 −1.0000000000000000	0.5861275452213199 −1.0000000000000000	0.3593519628863694 −1.0000000000000000
7	−0.7497222492047110 −0.7641686475074967	1.0000000000000000 −1.0000000000000000	0.8677139861534285 −1.0000000000000000	0.6718072968265310 −1.0000000000000000
8	0.7497222492047110 −0.7641686475074967	−0.8964006664142398 −0.9037747054613061	0.9981396004694932 −1.0000000000000000	0.8949872464334571 −1.0000000000000000
9	−0.6889822365046136 −0.6889822365046136	0.8964006664142398 −0.9037747054613061	−0.8246872285548802 −0.9699982047625423	1.0000000000000000 −1.0000000000000000
10	0.6889822365046136 −0.6889822365046136	−0.7930464008921687 −0.7930464008921687	0.8246872285548802 −0.9699982047625423	−0.9992591382562380 −0.9992591382562380
11	−0.3110177634953864 −0.3110177634953864	0.7930464008921687 −0.7930464008921687	−0.8641993803626567 −0.8641993803626567	0.9992591382562380 −0.9992591382562380
12	0.3110177634953864 −0.3110177634953864	−0.5000000000000000 −0.5000000000000000	0.8641993803626567 −0.8641993803626567	−0.8432145105568528 −0.9574614014591484
13	0.0000000000000000 0.0000000000000000	0.5000000000000000 −0.5000000000000000	−0.6308098017028516 −0.6308098017028516	0.8432145105568528 −0.9574614014591484
14		−0.2069535991078313 −0.2069535991078313	0.6308098017028516 −0.6308098017028516	−0.9207514598210227 −0.9207514598210227
15		0.2069535991078313 −0.2069535991078313	−0.3691901982971484 −0.3691901982971484	0.9207514598210227 −0.9207514598210227
16		0.0000000000000000 0.0000000000000000	0.3691901982971484 −0.3691901982971484	−0.7543814375798548 −0.7568093664013312
17			−0.1358006196373433 −0.1358006196373433	0.7543814375798548 −0.7568093664013312
18			0.1358006196373433 −0.1358006196373433	−0.7249538986620887 −0.7249538986620887
19				0.7249538986620887 −0.7249538986620887
20				−0.2750461013379113 −0.2750461013379113
21				0.2750461013379113 −0.2750461013379113
22				−0.0635342636473669 −0.1156087916821725
23				0.0635342636473669 −0.1156087916821725
24				−0.0792485401789773 −0.0792485401789773
25				0.0792485401789773 −0.0792485401789773
26				0.0000000000000000 −0.0165548344873347
27				−0.0007408617437620 −0.0007408617437620
28				0.0007408617437620 −0.0007408617437620
29				0.0000000000000000 0.0000000000000000

Therefore, we need to determine only superconvergent points in $\hat{T}_1$. Superconvergence in $\hat{T}_2$ are obtained by symmetry. TABLE 3 demonstrates function value superconvergent points in $\hat{T}_1$ for $n = 1, \ldots, 8$ with 16 digits of accuracy. The contours $\psi_{n+1}^{Re} = 0$ and $\psi_{n+1}^{Im} = 0$ for $n = 1, \ldots, 8$ are given in FIGURE 14 and FIGURE 15.

We now apply Theorem 3.2 in derivative superconvergence to the Laplace equation. For

TABLE 4. x-Derivative Superconvergent Points for the Criss-Cross Pattern (in $\hat{T}_1$, $n = 1, \ldots, 8$)

	$n=1$	$n=2$	$n=3$	$n=4$
1	0.0000000000000000 −1.0000000000000000	−0.5773502691896258 −1.0000000000000000	−0.7071067811865475 −1.0000000000000000	−0.8477823441259478 −1.0000000000000000
2		0.5773502691896258 −1.0000000000000000	0.0000000000000000 −1.0000000000000000	−.32045852838843981 −1.0000000000000000
3			0.7071067811865475 −1.0000000000000000	0.3204585283884398 −1.0000000000000000
4			0.0000000000000000 0.0000000000000000	0.8477823441259478 −1.0000000000000000
5				0.0000000000000000 −0.0224627212127888

	$n=5$	$n=6$	$n=7$	$n=8$
1	−0.9022588235195235 −1.0000000000000000	−0.9310770981941091 −1.0000000000000000	−0.9465714662683107 −1.0000000000000000	−0.9588192910578902 −1.0000000000000000
2	−0.5288468732829620 −1.0000000000000000	−0.6566413396532959 −1.0000000000000000	−0.7373956542010889 −1.0000000000000000	−0.7924029133810774 −1.0000000000000000
3	0.0000000000000000 −1.0000000000000000	−0.2356824218715548 −1.0000000000000000	−0.4022593795202400 −1.0000000000000000	−0.5215086649681956 −1.0000000000000000
4	0.5288468732829620 −1.0000000000000000	0.2356824218715548 −1.0000000000000000	0.0000000000000000 −1.0000000000000000	−0.1817673913302495 −1.0000000000000000
5	0.9022588235195235 −1.0000000000000000	0.6566413396532959 −1.0000000000000000	0.4022593795202400 −1.0000000000000000	0.1817673913302495 −1.0000000000000000
6	0.0000000000000000 0.0000000000000000	0.9310770981941091 −1.0000000000000000	0.7373956542010889 −1.0000000000000000	0.5215086649681956 −1.0000000000000000
7		−0.0891940958115766 −0.1171153414673580	0.9465714662683107 −1.0000000000000000	0.7924029133810774 −1.0000000000000000
8		0.0891940958115766 −0.1171153414673580	−0.0382832107422798 −0.0748454610760943	0.9588192910578902 −1.0000000000000000
9			0.0382832107422798 −0.0748454610760943	−0.9264627610278532 −0.9700802098022849
10			0.0000000000000000 0.0000000000000000	0.9264627610278532 −0.9700802098022849
11				−0.1589910559373525 −0.1863775498631390
12				0.1589910559373525 −0.1863775498631390
13				0.0000000000000000 −0.1134648999929049
14				−0.0418841026400703 −0.0612506331535669
15				0.0418841026400703 −0.0612506331535669
16				0.0000000000000000 −0.0007334155159263

x-derivative superconvergence, we need to determine the common zeros of $\frac{\partial \psi_{n+1}^{Re}}{\partial x} = 0$ and $\frac{\partial \psi_{n+1}^{Im}}{\partial x} = 0$ in both $\hat{T}_1$ and $\hat{T}_2$, since (3.28) does not imply any symmetric properties for x-derivatives.

We list superconvergent points for $n = 1, \ldots, 8$ in TABLE 4 and TABLE 5 with 16 digits of accuracy. Only the contours $\frac{\partial \psi_{n+1}^{Re}}{\partial x} = 0$ and $\frac{\partial \psi_{n+1}^{Im}}{\partial x} = 0$ for $n = 3, \ldots, 8$ are given in FIGURE 16.

On the other hand, from (3.28), the y-derivatives of ψ_{n+1}^{Re} and ψ_{n+1}^{Im} are symmetric to the x-derivatives. Thus, the y-derivative superconvergent points can be obtained by symmetry.

Remark 3.13. To compare our results with those given in [2] [5], we use $\tilde{x} = (x+1)/2$ and

[5] Derivative superconvergent points are given for $n = 1, \ldots, 6$ in [2] (TABLE II, III).

TABLE 5. x-Derivative Superconvergent Points for the Criss-Cross Pattern (in $\hat{T}_2$, $n = 1, \ldots, 8$)

	$n=1$	$n=2$	$n=3$	$n=4$
1	0.0000000000000000 0.0000000000000000	0.5773502691896258 0.0000000000000000	0.0000000000000000 0.0000000000000000	0.5242840088938378 −0.3672919579081908
2			0.7500000000000000 −0.4330127018922193	0.5242840088938378 0.3672919579081908
3			0.7500000000000000 0.0000000000000000	0.7941585351606128 0.0000000000000000
4			0.7500000000000000 0.4330127018922193	0.8291726306727321 −0.2066731091555382
5				0.8291726306727321 0.2066731091555382

	$n=5$	$n=6$	$n=7$	$n=8$
1	0.0000000000000000 0.0000000000000000	0.4172857146226821 0.0000000000000000	0.0000000000000000 0.0000000000000000	0.0094266635593945 0.0000000000000000
2	0.3766028903116235 −0.2436531088238106	0.5263929773620074 −0.4332798971957640	0.5355367828576363 −0.2200378052788761	0.0673857238109867 −0.0421135710689382
3	0.3766028903116235 0.2436531088238106	0.5263929773620074 0.4332798971957640	0.5355367828576363 0.2200378052788761	0.0673857238109867 0.0421135710689382
4	0.5081763283085686 −0.3204147860450027	0.6569757558957244 −0.2092748096819668	0.6438730997258771 −0.5724579277550955	0.5853163679868406 0.0000000000000000
5	0.5081763283085686 0.3204147860450027	0.6569757558957244 0.2092748096819668	0.6438730997258771 0.5724579277550955	0.6496603573416232 −0.3920199824799846
6	0.5520845860159235 0.0000000000000000	0.6665389441764509 0.0000000000000000	0.7289644770413350 0.0000000000000000	0.6496603573416232 0.3920199824799846
7	0.5623467631434243 −0.0834391002091283	0.6766532889073166 −0.2597018851468181	0.9150910586863469 0.0000000000000000	0.7164981840772373 −0.6611375478929451
8	0.5623467631434243 0.0834391002091283	0.6766532889073166 0.2597018851468181		0.7164981840772373 0.6611375478929451
9	0.6737396038956180 −0.5463668183039467	0.7016063317069908 −0.5860557493229441		0.7687927787500516 0.0000000000000000
10	0.6737396038956180 0.5463668183039467	0.7016063317069908 0.5860557493229441		0.9271673933371417 0.0000000000000000
11	0.8669379104781077 0.0000000000000000	0.7356517149502489 −0.6300926285368980		
12		0.7356517149502489 0.6300926285368980		
13		0.8935538681815075 0.0000000000000000		

$\tilde{y} = (y+1)/2$ to map elements $\hat{T}_1$ and $\hat{T}_2$ to elements τ_1 and τ_2 in [2], respectively. The superconvergent points in $\hat{T}_i$ are also mapped to the superconvergent points in τ_i, $i = 1, 2$ (see Remark 3.5 for reasons). Almost all of the points in [2] are accurate in 10 digits. However, in case $n = 3$, the y-coordinates of the second and the fourth points in τ_2 are 0.2834936534 and 0.7165063710, which are accurate in 8 and 7 digits, respectively. By our process, these two points can be located analytically, which are $(4 \pm \sqrt{3})/8$ (after mapped into τ_2), or 0.2834936490538904 and 0.7165063509461097 in decimals. □

References

[1] A.B. Andreev and R.D. Lazarov, *Superconvergence of the gradient for quadratic triangular finite element methods*, Numer. Meth. PDEs 4 (1988), 15-32.

[2] I. Babuška, T. Strouboulis, C.S. Upadhyay, and S.K. Gangaraj, *Computer-based proof of the existence of superconvergence points in the finite element method; superconver-*

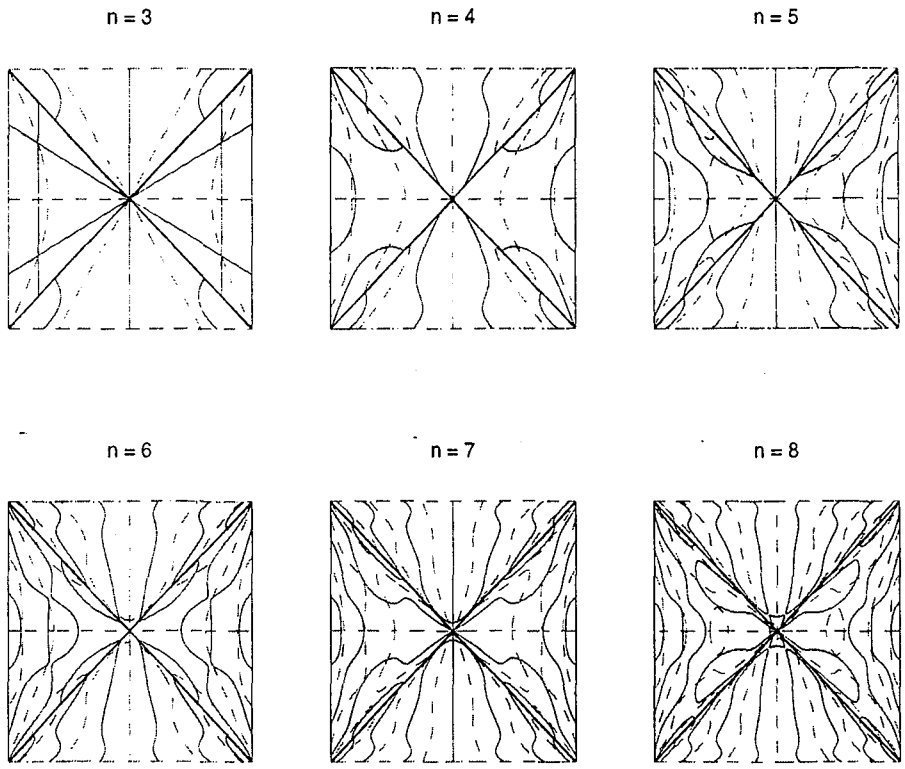

Figure 16: Contours $\frac{\partial \psi_{n+1}^{Re}}{\partial x} = 0$ (solid) and $\frac{\partial \psi_{n+1}^{Im}}{\partial x} = 0$ (dashed), $n = 3, \ldots, 8$.

gence of the derivatives in finite element solutions of Laplace's, Poisson's, and the elasticity equations, Numer. Meth. PDEs. **12** (1996), 347-392.

[3] I. Babuška and T. Strouboulis, *The Finite Element Method and its Reliability*, Oxford University Press, London, 2001.

[4] C.M. Chen, *Structure Theory of Superconvergence of Finite Elements* (in Chinese), Hunan Science Press, China, 2001.

[5] C.M. Chen and Y.Q. Huang, *High Accuracy Theory of Finite Element Methods* (in Chinese). Hunan Science Press, China, 1995.

[6] J. Douglas Jr. and T. Dupont, *Superconvergence for Galerkin methods for the two point boundary problem via local projections*, Numer. Math. **21** (1973), 270-278.

[7] R.E. Ewing, R.D. Lazarov, and J. Wang, *Superconvergence of the velocity along the Gauss lines in mixed finite element methods*, SIAM J. Numer. Anal. **28** (1991), 1015-1029.

[8] J.D. Faires and R. Burden, *Numerical Methods*, 2nd edition, Brooks/Cole Publishing Company, Pacific Grove, 1998.

[9] M. Křížek, P. Neittaanmäki, and R. Stenberg (Eds.) *Finite Element Methods: Superconvergence, Post-processing, and A Posteriori Estimates*, Lecture Notes in Pure and Applied Mathematics Series, Vol.196, Marcel Dekker, New York, 1997.

[10] P. Lesaint and M. Zlámal, *Superconvergence of the gradient of finite element solutions*, RAIRO Anal. Numér. **13** (1979), 139-166.

[11] Q. Lin and J. Xu. *Linear finite elements with high accuracy*, J. Comp. Math. **3** (1985), 115–133.

[12] Q. Lin and N. Yan, *Construction and Analysis of High Efficient Finite Elements* (in Chinese), Hebei University Press, China, 1996.

[13] R. Lin, *Doctoral Dissertation*, to appear.

[14] A.H. Schatz, I.H. Sloan, and L.B. Wahlbin, *Superconvergence in finite element methods and meshes that are locally symmetric with respect to a point*, SIAM J. Numer. Anal. **33** (1996), 505-521.

[15] A.H. Schatz and L.B. Wahlbin, *Interior maximum norm estimates for finte element methods. Part II*, Math. Comp. **64** (1995), 907-928.

[16] B. Szabó and I. Babuška, *Finite Element Analysis*, John Wiley & Sons, New York, 1991.

[17] L.B. Wahlbin, *Superconvergence in Garlerkin Finite Element Methods*, Lecture Notes in Mathematics, Vol. 1605, Springer, Berlin, 1995.

[18] Z. Zhang, *Derivative superconvergence points in finite element solutions of Poisson's equation for the serendipity and intermediate families – A theoretical justification*, Math. Comp. **67** (1998), 541-552.

[19] Z. Zhang, *Derivative superconvergent points in finite element solutions of harmonic functions – A theoretical justification*, Math. Comp. **71** (2002), 1421-1430.

[20] Q.D. Zhu and Q. Lin, *Superconvergence Theory of the Finite Element Method* (in Chinese), Hunan Science Press, China, 1989.